

Sparse Generalized Yule–Walker Estimation for Large Spatio-temporal Autoregressions with an Application to NO₂ Satellite Data

Hanno Reuvers¹ and Etienne Wijler²

¹Department of Econometrics, Erasmus University Rotterdam, 3062 PA Rotterdam, The Netherlands

²Department of Quantitative Economics, Maastricht University, 6200 MD Maastricht, The Netherlands

August 9, 2021

Abstract

We consider sparse estimation of a class of high-dimensional spatio-temporal models. Unlike classical spatial autoregressive models, we do not rely on a predetermined spatial interaction matrix. Instead, under the assumption of sparsity, we estimate the relationships governing both the spatial and temporal dependence in a fully data-driven way by penalizing a set of Yule-Walker equations. While this regularization can be left unstructured, we also propose a customized form of shrinkage to further exploit diagonally structured forms of sparsity that follow intuitively when observations originate from spatial grids such as satellite images. We derive finite sample error bounds for this estimator, as well estimation consistency in an asymptotic framework wherein the sample size and the number of spatial units diverge jointly. A simulation exercise shows strong finite sample performance compared to competing procedures. As an empirical application, we model satellite measured NO₂ concentrations in London. Our approach delivers forecast improvements over a competitive benchmark and we discover evidence for strong spatial interactions between sub-regions.

1 Introduction

Spatial econometrics provides models to describe the cross-sectional dependence among entities observed at different locations. A key quantity is the so-called spatial weight matrix. Parametric choices for this spatial weight matrix, e.g. adjacency matrix, inverse physical distance and spatial contiguity weights, are very popular and give rise to interesting spatial models and novel estimation techniques. The formulation of these spatial models typically involves two steps. First, the product of the spatial weight matrix and the vector of the contemporaneous observations is constructed to create a spatial lag. Second, spatial dependencies are modeled by augmenting an existing econometric model with the spatial lag. The necessity for dedicated estimation techniques

stems from the endogeneity problem caused by the contemporaneous variable appearing simultaneously in the dependent variable and in the spatial lag. Examples of this two-step approach include: the spatial autoregressive model (a linear regression model with spatial lag) with a Gaussian quasi-maximum likelihood estimator (QMLE), see e.g. Lee (2004); the QMLE estimation of stationary spatial panel with fixed effects detailed in Yu et al. (2008); the extension of these spatial panels to include spatially autoregressive disturbances as in Lee and Yu (2010); Yu et al. (2012) cover a non-stationary case where units can be spatially cointegrated; and the computationally beneficial generalized method of moments (GMM) estimator by Lee and Yu (2014). Possible application areas for spatial econometric models are wide-spread. A non-exhaustive list of examples include product demand across U.S. states, pollution concentrations across measurement sites, housing prices with location information, co-movement between stock indices, and interactions between social network users have all been studied using spatial econometric methods.

The choice of the spatial weight matrix is a key element of the model specification. Nevertheless, it also involves a selection process that can feel somewhat arbitrary and/or tedious. The arbitrariness might prevail when practical considerations fail to suggest a particular mechanism for the spatial interactions. Alternatively, in large data sets with many spatial sites, there are simply too many spatial interactions to be modeled. Two solutions have been proposed in the literature. First, there is the option to use multiple weight matrices. These weight matrices can be combined through either a convex combination (see, e.g. Debarsy and LeSage (2018)) or a model averaging approach as in Zhang and Yu (2018). Second, at the expense of estimating many parameters, we might decide to directly infer the spatial interactions from the data. In both cases, the estimation method has to account for the endogeneity issue.

We propose the SPatial LAsso-type SHrinkage (SPLASH) estimator. Building upon previous works by Dou et al. (2016) and Gao et al. (2019), we study spatio-temporal regressions. Apart from a more generous bandwidth upper bound, this SPLASH estimator leaves the spatial weight matrix and autoregressive matrix unspecified while employing a lasso approach to recover sparse solutions. The endogeneity problem is resolved by using an estimator which solves the generalized Yule-Walker equations. We make five contributions. First, assuming sparsity in the coefficient matrices and general mixing conditions on the innovations, we derive finite-sample performance bounds for the estimation and prediction error of our estimator. We subsequently utilize these bounds to derive asymptotic consistency in a variety of settings. For example, in the special case of a finite bandwidth and unstructured sparsity, it is demonstrated that the number of spatial units N may grow at any polynomial rate of the number of temporal observations T . Second, we adopt a banded estimation procedure for the autocovariance matrices that underlie the generalized Yule-Walker equations. The faster convergence rates of these banded autocovariance matrix estimators are shown to translate into better convergence rates of our SPLASH estimator. Third, we show that dependence between neighbouring units that are ordered on a spatial grid translates to diagonally structured forms of sparsity in the spatial weight matrix, for which we develop a tailored regularization procedure reminiscent of the sparse group lasso. Fourth and final, we consider an empirical application in which we employ SPLASH to predict NO_2 concentrations in London based on satellite data.

Elaborating on the empirical application, we collect daily NO_2 column densities from August 2018 to October 2020, recorded by the TROPOspheric Monitoring Instrument (TROPOMI) on board of the Copernicus Sentinel-5 Precursor satellite. Each spatial unit in this application corresponds to an aggregation of a small number of pixels on the satellite image. We find that SPLASH constructs more accurate one-step ahead predictions for all spatial units compared to the procedure in Gao et al. (2019), while outperforming a competitive penalized VAR benchmark for the majority

of spatial units. In addition, we find evidence for spatial interactions between first-order neighbours and second-order neighbours (i.e. neighbours of neighbours).

There are two strands of literature that are closely linked to this work: the literature on the estimation of (nonparametric) spatial weight matrices and the literature on spatio-temporal vector autoregressions. Some similarities and differences are as follows. Lam and Souza (2014) consider a model specification where the spatial units depend linearly on a spatial lag and a set of exogenous regressors. The adaptive lasso is proven to select the correct sparsity pattern. To solve the endogeneity issue, they require the error variance to decay to zero as the time dimension grows large. Ahrens and Bhattacharjee (2015) solve the endogeneity problem using external instruments. Their two-step lasso estimation procedure selects the relevant instruments in the first step and the relevant spatial interactions in the second step. The theoretical properties of this estimator are derived using moderate deviation theory as in Jing et al. (2003). This approach requires the instruments and the idiosyncratic component to be serially independent. Clearly, a serial independence assumption is unrealistic for the spatio-temporal models we consider here. Finally, Lam and Souza (2019) augment a spatial lag model with a set of potentially endogenous variables (the augmenting set). They decompose the spatial weight matrix into a pre-determined component based on expert knowledge and a sparse adjustment matrix that represents specification errors. The adjustment matrix is sparsely estimated based on a penalized version of instrumental variables (IV) regression. If these instrumental variables are selected as temporal lags of the dependence variable, then their IV regressions are similar to generalized Yule-Walker estimation. In contrast to our approach, Lam and Souza (2019) do not regularize the interactions between the dependent variables and the variables in the augmenting set, and they assume the number of such interactions to be fixed. A fixed number of interactions is inappropriate in high-dimensional settings in which the number of spatial units is allowed to diverge.

Most closely related to the work presented in this paper are Gao et al. (2019), and Ma et al. (2021). Both of these paper consider the same model and an estimation procedure that relies on the generalized Yule-Walker equations. The key difference with our paper lies in the method by which the model complexity is controlled during estimation. Gao et al. (2019) assume the coefficient matrices to be banded with a bandwidth that is small in relation to the number of spatial units. The bandwidth is determined from the data and all parameters within the selected bandwidth are left unregularized. Our SPLASH estimator, however, has the ability to exploit (structured) sparsity within the bandwidth and thereby improve estimation and forecasting performance. In addition, after imposing a general upper bound on the bandwidth to ensure identification, no a priori choice regarding the bandwidth is required when using SPLASH. The recently developed bagging approach in Ma et al. (2021) does allow for sparsity within the bands, yet it also requires the calculation of so-called solution paths. That is, a forward addition and backward deletion stage are needed to determine the variables that enter the final model specification. In contrast, the SPLASH estimator provides this solution at once. Furthermore, their approach is not designed to detect diagonally structured forms of sparsity, while the ability to do so results in clear performance improvements of SPLASH in both the simulations and the empirical application considered below.

This paper is organized as follows. Section 2 introduces the spatio-temporal vector autoregression and the banded autocovariance estimator that underlies the generalized Yule-Walker estimation approach. The SPLASH estimator and its theoretical properties are discussed in Section 3. The simulation results in Section 4 and the empirical application in Section 5 demonstrate the benefits of the SPLASH estimator. Section 6 concludes.

Notation

The indicator function $\mathbb{1}_{\{A\}}$ equals 1 if A is true and zero otherwise. For a vector $\mathbf{x} \in \mathbb{R}^N$, the L_p -norm of \mathbf{x} is denoted $\|\mathbf{x}\|_p = (\sum_{i=1}^N |x_i|^p)^{1/p}$, with $\|\mathbf{x}\|_\infty = \max_i |x_i|$ as an important special case. The total number elements in \mathbf{x} is denoted by $|\mathbf{x}|$, while the number of non-zero elements in \mathbf{x} is denoted by $\mathcal{M}(\mathbf{x}) = \sum_{i=1}^N \mathbb{1}\{x_i \neq 0\}$. The Orlicz norm is defined as $\|\cdot\|_\psi = \inf\{c > 0 : \mathbb{E}[\psi(|\cdot|/c)] \leq 1\}$ for any $\psi(\cdot) : \mathbb{R}^+ \rightarrow \mathbb{R}^+$ being a convex, increasing function with $\psi(0) = 0$ and $\psi(x) \rightarrow \infty$ as $x \rightarrow \infty$. In addition, we rely on several types of matrix norms. For a matrix $\mathbf{A} \in \mathbb{R}^{M \times N}$, the matrix norms induced by the vector L_p -norms are given by $\|\mathbf{A}\|_p = \sup_{\mathbf{x} \in \mathbb{R}^M} (\|\mathbf{A}\mathbf{x}\|_p / \|\mathbf{x}\|_p)$. Noteworthy examples are: $\|\mathbf{A}\|_1 = \max_{1 \leq j \leq N} \sum_{i=1}^M |a_{ij}|$, the spectral norm $\|\mathbf{A}\|_2 = [\lambda_{\max}(\mathbf{A}'\mathbf{A})]^{1/2}$ where $\lambda_{\max}(\cdot)$ stands for the maximum eigenvalue, and $\|\mathbf{A}\|_\infty = \max_{1 \leq i \leq M} \sum_{j=1}^N |a_{ij}|$. The Frobenius norm of \mathbf{A} is $\|\mathbf{A}\|_F = (\sum_{i=1}^M \sum_{j=1}^N |a_{ij}|^2)^{1/2}$. Finally, we define $\|\mathbf{A}\|_{\max} = \max_{i,j} |a_{ij}|$ and $\|\mathbf{A}\|_{\mp} = \max\{\|\mathbf{A}\|_1, \|\mathbf{A}\|_\infty\}$. Let $S \subseteq \{1, \dots, N\}$ denote an index set with cardinality denoted by $|S|$. Then, \mathbf{x}_S denotes the $|S|$ -dimensional vector with the elements of \mathbf{x} indexed by S , whereas \mathbf{A}_S denotes the $(M \times |S|)$ -dimensional matrix containing the columns of \mathbf{A} indexed by S . In addition, we define $\mathcal{D}_A(k) = \{a_{ij} \mid |i - j| = k\}$ as the collections of elements lying on (pairs of) the diagonals in the matrix \mathbf{A} . Finally, C is a generic constant that can change value from line-to-line.

2 The Spatio-temporal Vector Autoregression

As in the recent paper by Gao et al. (2019), we consider the spatio-temporal vector autoregression

$$\mathbf{y}_t = \mathbf{A}\mathbf{y}_t + \mathbf{B}\mathbf{y}_{t-1} + \boldsymbol{\epsilon}_t, \quad t = 1, \dots, T, \quad (1)$$

where $\mathbf{y}_t = (y_{1t}, \dots, y_{Nt})'$ stacks the observations at time t over a collection of N spatial units. The contemporaneous spatial dependence between these spatial units is governed by the matrix $\mathbf{A} = (a_{ij})_{i,j=1}^N$ with $a_{ii} = 0$ for $i = 1, \dots, N$. The matrix $\mathbf{B} = (b_{ij})_{i,j=1}^N$ incorporates dependence on past realizations. Finally, we have the innovation vector $\boldsymbol{\epsilon}_t$. We impose the following assumptions on the DGP in (1).

Assumption 1 (Stability).

(a) $\|\mathbf{A}\|_{\mp} = \max\{\|\mathbf{A}\|_1, \|\mathbf{A}\|_\infty\} \leq \delta_A < 1$.

(b) $\|\mathbf{B}\|_{\mp} \leq C_B$ and $\frac{C_B}{1 - \delta_A} < 1$.

Remark 1. Assumption 1 is defined in terms of $\|\cdot\|_{\mp}$. Since $\|\mathbf{A}\|_1 = \|\mathbf{A}'\|_\infty \leq \|\mathbf{A}\|_{\mp}$ for any matrix \mathbf{A} , the norm $\|\cdot\|_{\mp}$ is convenient when bounding products of matrices containing transposes.

Assumption 2 (Innovations).

- (a) The sequence $\{\boldsymbol{\epsilon}_t\}$ is a covariance stationary, martingale difference process with respect to the filtration $\mathcal{F}_{t-1} = \sigma(\boldsymbol{\epsilon}_{t-1}, \boldsymbol{\epsilon}_{t-2}, \dots)$, and geometrically strong mixing (α -mixing). That is, the mixing coefficients $\{\alpha_m\}$ satisfy $\alpha_m \leq c_2 e^{-\gamma_\alpha m}$ for all m and some constants $c_2, \gamma_\alpha > 0$. The largest and smallest eigenvalues of $\boldsymbol{\Sigma}_\epsilon = \mathbb{E}(\boldsymbol{\epsilon}_1 \boldsymbol{\epsilon}_1') = (\sigma_{ij})_{i,j=1}^N$ are bounded away from 0 and ∞ , uniformly in $T \in \mathbb{N}$.

(b) Either one of the following assumptions holds:

- (b1) For $\psi(x) = x^d$, we require $\sup_{i,t} \|\epsilon_{it}\|_\psi = (\mathbb{E}|\epsilon_{it}|^d)^{1/d} \leq \mu_d < \infty$ for $d \geq 4$.
- (b2) For $\psi(x) = \exp(x) - 1$, we have $\sup_{i,t} \|\epsilon_{it}\|_\psi \leq \mu_\infty < \infty$.

Assumption 1 ensures that $\mathbf{y}_t = \mathbf{A}\mathbf{y}_t + \mathbf{B}\mathbf{y}_{t-1} + \boldsymbol{\epsilon}_t$ has a stable reduced form VAR(1) specification. This follows from the following two observations. First, Assumption 2(a) bounds the maximum row and column sums of \mathbf{A} and thereby constraints the contemporaneous dependence between the time series. This assumption reminds of the spatial econometrics literature in which the spatial parameter λ is bounded from above and the prespecified spatial weight matrix \mathbf{W}_N is standardized (see, e.g. Lee (2004) and Lee and Yu (2010)). Typically, the product $\lambda\mathbf{W}_N$, the natural counter part of the matrix \mathbf{A} , is required to fulfil conditions similar to $\|\mathbf{A}\|_{\text{F}} \leq \delta_A < 1$.¹ Invertibility of $\mathbf{I}_N - \mathbf{A}$ is also guaranteed because $\|\mathbf{A}\|_2 \leq \sqrt{\|\mathbf{A}\|_1 \|\mathbf{A}\|_\infty} \leq \delta_A \leq 1$ and we have the reduced-form representation $\mathbf{y}_t = \mathbf{C}\mathbf{y}_{t-1} + \mathbf{D}\boldsymbol{\epsilon}_t$ with $\mathbf{C} = (\mathbf{I}_N - \mathbf{A})^{-1}\mathbf{B}$ and $\mathbf{D} = (\mathbf{I}_N - \mathbf{A})^{-1}$. From $\|\mathbf{D}\|_{\text{F}} \leq \sum_{j=0}^{\infty} \|\mathbf{A}\|_{\text{F}}^j = \frac{1}{1-\delta_A}$, we infer that the absolute row and column sum of $\mathbf{I}_N - \mathbf{A}$ are bounded. The latter is the logical counterpart of assumption B2 in Dou et al. (2016). Second, Assumption 2(b) controls serial dependence. Indeed, we conclude from $\|\mathbf{C}\|_2 \leq \|\mathbf{C}\|_{\text{F}} \leq \frac{C_B}{1-\delta_A} < 1$ that both unit root and explosive behaviour of the reduced form specification are ruled out. The resulting stable VAR(1) representation is convenient to study the theoretical properties of our penalized estimator.

The assumptions on the innovation process $\{\boldsymbol{\epsilon}_t\}$, Assumption 2, are closely related to those in Masini et al. (2019). Assumption 2(a) places restrictions on the time series properties of the error term through martingale difference (m.d.) and mixing assumptions. The m.d. assumption implies that $\mathbb{E}(\boldsymbol{\epsilon}_t \mathbf{y}'_{t-j}) = \mathbf{0}$, while the mixing assumption controls the serial correlation in the data. Polynomial or exponential tail decay of the distribution of the innovations are imposed through Assumptions 2(b1) and 2(b2), respectively. The type of tail decay will directly influence the growth rates we can allow for N and T . The discussions on pages 4–8 of Masini et al. (2019) demonstrate that Assumption 2 allows for a wide range of innovation models.

Any further structure being absent, there are $(2N - 1)N$ unknown parameters in \mathbf{A} and \mathbf{B} to estimate. Three complications are encountered when estimating these parameters. First, if $\mathbf{A} \neq \mathbf{0}$, then \mathbf{y}_t occurs on both sides of the equation, and we face an endogeneity problem which renders the ordinary least squares estimator inconsistent. Second, the number of unknown parameters grows quadratically in the cross-sectional dimension N . The model thus quickly becomes too large to estimate accurately without regularization. Finally, the multitude of parameters raises concerns about identifiability. These three complications are addressed by: (1) imposing structure on the matrices \mathbf{A} and \mathbf{B} , and (2) estimating the unknown coefficients using the Yule-Walker equations (e.g. Brockwell and Davis, 1991, p. 420).

There are several possibilities to introduce structure into \mathbf{A} and/or \mathbf{B} . Early spatial econometrics models, e.g. the spatial autoregressive (SAR) model or spatial Durbin model (SDM), incorporate spatial effects through the product $\lambda\mathbf{W}_N$ (with \mathbf{W}_N pre-specified). The specification $\mathbf{A} = \lambda\mathbf{W}_N$ imposes substantial structure on \mathbf{A} and leaves only the single parameter λ to estimate. Dou et al. (2016) consider a more general setting in which each row of \mathbf{W}_N receives its own scale parameter. Specifically, they set $\mathbf{A} = \text{diag}(\boldsymbol{\lambda}_0)\mathbf{W}_N$ and $\mathbf{B} = \text{diag}(\boldsymbol{\lambda}_1) + \text{diag}(\boldsymbol{\lambda}_2)\mathbf{W}_N$, and estimate

¹For instance, it is not uncommon to row-normalize \mathbf{W}_N (each absolute row sum equal to 1) and restrict $\lambda < 1$, see pages 1903-1904 of Lee (2004). If \mathbf{W}_N is symmetric, then also $\|\lambda\mathbf{W}_N\|_{\text{F}} < 1$.

the $3N$ coefficients in $(\boldsymbol{\lambda}'_0, \boldsymbol{\lambda}'_1, \boldsymbol{\lambda}'_2)'$. Gao et al. (2019) require \mathbf{A} and \mathbf{B} to be banded matrices.² We employ a similar assumption.

Assumption 3 (Banded matrices). Recall $\mathbf{A} = (a_{ij})_{i,j=1}^N$, $\mathbf{B} = (b_{ij})_{i,j=1}^N$, and $\boldsymbol{\Sigma}_\epsilon = (\sigma_{ij})_{i,j=1}^N$. We have: (a) $a_{ij} = b_{ij} = 0$ for all $|i - j| > k$ with $k < \lfloor N/4 \rfloor$, and (b) $\sigma_{ij} = 0$ for all $|i - j| > l_0$.

Assumption 3 serves two purposes. First, for each spatial unit $i = 1, \dots, N$, the matrices \mathbf{A} and \mathbf{B} are banded to have no more than N unknown parameters per equation. With N moment conditions for each i , Assumption 3(a) is key in identifying the parameters. Our discussions in Section 3 illustrate that this assumption is realistic when the data is observed on a regular grid. The combination of Assumptions 3(a)–(b) is exploited in the Yule-Walker estimation approach. This approach requires estimation of the $(N \times N)$ autocovariance matrices $\boldsymbol{\Sigma}_j = \mathbb{E}(\mathbf{y}_t \mathbf{y}'_{t-j})$. Especially in our large N settings, it is crucial to rely on covariance matrix estimators that converge at a fast rate. If \mathbf{A} , \mathbf{B} , and $\boldsymbol{\Sigma}_\epsilon$ are banded, then the following result applies.

Theorem 1 (Convergence rates for banded sample autocovariance matrices). *For any matrix $\mathbf{M} = (m_{ij})$, its h -banded counterpart is defined as $\mathcal{B}_h(\mathbf{M}) = (m_{ij} \mathbb{1}_{\{|i-j| \leq h\}})$. Define the $(N \times 2N)$ matrix $\hat{\mathbf{V}}_h = [\mathcal{B}_h(\hat{\boldsymbol{\Sigma}}_1)' \ \mathcal{B}_h(\hat{\boldsymbol{\Sigma}}_0)]$ with $\hat{\boldsymbol{\Sigma}}_1 = \frac{1}{T} \sum_{t=2}^T \mathbf{y}_t \mathbf{y}'_{t-1}$ and $\hat{\boldsymbol{\Sigma}}_0 = \frac{1}{T} \sum_{t=2}^T \mathbf{y}_t \mathbf{y}'_t$, and choose*

$$h = h(\epsilon, N) = \left(\frac{\log(C_4 N / \epsilon)}{|\log(\delta_C)|} + 1 \right) \left(3 \max \left\{ s^*, \frac{\log(C_4 N / (1 - \delta_C) \epsilon)}{|\log(\delta_A)|} \right\} + 1 \right) k_0 + 6 \max \left\{ s^*, \frac{\log(C_4 N / (1 - \delta_C) \epsilon)}{|\log(\delta_A)|} \right\} k_0 + l_0, \quad (2)$$

then $\|\hat{\mathbf{V}}_h - \mathbf{V}\|_{\text{F}} \leq 6\epsilon$ with a probability of at least

(a) $1 - 2\mathcal{P}_1(\epsilon, N, T)$ under Assumptions 1–3 using Assumption 2(b1) (polynomial tails),

(b) $1 - 2\mathcal{P}_2(\epsilon, N, T)$ under Assumptions 1–3 using Assumption 2(b2) (exponential tails),

where

$$\mathcal{P}_1(\epsilon, N, T) = N^2 \left[\left(b_1 T^{(1-\delta)/3} + \frac{[2h(\epsilon, N) + 1] b_3}{\epsilon} \right) \exp \left(-\frac{T^{(1-\delta)/3}}{2b_1^2} \right) + \frac{b_2 [2h(\epsilon, N) + 1]^d}{\epsilon^d T^{\frac{\delta}{2}(d-1)}} \right],$$

for some $0 < \delta < 1$, and

$$\mathcal{P}_2(\epsilon, N, T) = N^2 \left[\frac{\beta_1 [2h(\epsilon, N) + 1]}{\epsilon} + \frac{2}{\beta_2} \left(\frac{T\epsilon^2}{[2h(\epsilon, N) + 1]^2} \right)^{\frac{1}{7}} \right] \exp \left(-\frac{1}{\beta_3} \left(\frac{T\epsilon^2}{[2h(\epsilon, N) + 1]^2} \right)^{\frac{1}{7}} \right).$$

All constants (C_4 , δ_C , s^* , etc.) are positive and independent of N and T . The proof (see the Appendix) shows how these constants are related to quantities in Assumptions 1–3.

Theorem 1 shows that banded estimators for $\boldsymbol{\Sigma}_0$ and $\boldsymbol{\Sigma}_1$ can provide an accurate approximation to $\mathbf{V} = [\boldsymbol{\Sigma}'_1 \ \boldsymbol{\Sigma}_0]'$. Each of these banded matrices has at most $2h(\epsilon, N) + 1$ nonzero elements in their columns/rows. For fixed ϵ , the term $2h(\epsilon, N) + 1 = O([\log(N/\epsilon)]^2)$ increases at a rate much slower than N^2 . This will eventually lead to better convergence rates for our SPLASH estimator.

²We say that the matrix \mathbf{A} has bandwidth k if the total number of nonzero entries in the any row or column is at most k . In other words, if the matrix \mathbf{A} satisfies $a_{ij} = 0$ for all $|i - j| > k$, then \mathbf{A} has a bandwidth of $2k + 1$ (at most).

3 Sparse Estimation

3.1 The SPLASH(α, λ) Estimator

The matrices \mathbf{A} and \mathbf{B} in (1) contain a total of $2N(N - 1)$ parameters. For large N , the accurate estimation of all these parameters becomes infeasible rather quickly. To alleviate this curse of dimensionality, we rely on sparsity. Some sparsity has been imposed already through Assumption 3 which was made for identifiability purposes. But this only partially solves the issue, since the number of parameters continues to grow quadratically in N . Further dimension reductions are possible whenever the spatial units are ordered in a structured way.

As an illustrative example, let us consider repeated measurements on the (5×5) spatial grids shown in the left column of Figure 1. The $N = 25$ spatial units are labelled y_1 up to y_{25} and enumerated row-wise. This ordering of the spatial entities creates an implicit notion of proximity and we intuitively expect economic and/or physical interactions to be most pronounced at short length scales. In Figure 1(a) we depart from the situation in which the spatial units are restricted to communicate horizontally. Blue arrows indicate explicitly that y_1 interacts with y_2 , and y_{14} interacts with both y_{13} and y_{15} . Of course, such interactions will occur among all elements in the grid. More importantly, if only these horizontal interaction exist, then the (25×25) matrices \mathbf{A} and \mathbf{B} feature a sparsity pattern as shown in Figure 1(b). The blue elements are potentially nonzero whereas uncolored elements are zero. The nonzero elements in \mathbf{A} and \mathbf{B} are thus clustered in specific, dense diagonals with the occasional zero when horizontal neighbours are absent (i.e. on the boundary of the grid). The diagonal nature of the sparsity is not an artifact of allowing horizontal interactions only. Figures 1(c) adds the vertical interactions and the accompanying sparsity pattern again manifests itself along diagonals (Figure 1(d)). Finally, with diagonal nearest neighbours being horizontal neighbors of vertical elements, we observe a “thickening” of the diagonals in Figure 1(f). Guided by these considerations we combine generalized Yule-Walker estimation with a sparse group penalty (e.g. Simon et al., 2013). The Yule-Walker estimator will control for endogeneity. The sparse group penalty will shrink towards diagonal structures by including/omitting complete diagonals and thus selecting the required interactions. Compared to Gao et al. (2019), we hereby gain the ability to exploit sparsity within banded matrices.

A formal definition of our estimator requires further notation. Part of this notation comes naturally if we briefly review the generalized Yule-Walker estimator. After post-multiplying by \mathbf{y}'_{t-1} and taking expectations, we find $\boldsymbol{\Sigma}'_1 = \mathbf{A}\boldsymbol{\Sigma}'_1 + \mathbf{B}\boldsymbol{\Sigma}'_0$ or, equivalently,

$$\boldsymbol{\Sigma}'_1 = [\boldsymbol{\Sigma}'_1 \quad \boldsymbol{\Sigma}'_0] [\mathbf{A} \quad \mathbf{B}]' =: \mathbf{V}\mathbf{C}'. \quad (3)$$

The i^{th} column of \mathbf{C}' contains all coefficients that belong to the i^{th} equation in (1). Assumption 3 requires several of these coefficients to be zero so we exclude these from the outset. We collect all remaining (possibly) nonzero coefficients in the i^{th} equation in the vector \mathbf{c}_i , and define \mathbf{V}_i as the matrix containing the corresponding columns from \mathbf{V} . In the population, we have $\mathbf{V}_i\mathbf{c}_i = \boldsymbol{\Sigma}'_1\mathbf{e}_i =: \boldsymbol{\sigma}_i$ for $i = 1, \dots, N$. Sample counterparts of \mathbf{V}_i and $\boldsymbol{\sigma}_i$ are readily available from the sample autocovariance matrices. More explicitly, Gao et al. (2019) set $\hat{\boldsymbol{\sigma}}_i = \frac{1}{T} \sum_{t=2}^T \mathbf{y}_{t-1}y_{it}$ and construct $\hat{\mathbf{V}}_i$ from the appropriate columns of $\hat{\mathbf{V}} = [\hat{\boldsymbol{\Sigma}}'_1 \quad \hat{\boldsymbol{\Sigma}}'_0]$. Motivated by $\boldsymbol{\sigma}_i - \mathbf{V}_i\mathbf{c}_i = \mathbf{0}$, they define the estimator $\hat{\mathbf{c}}_i$ as the following minimizer:

$$\hat{\mathbf{c}}_i = \arg \min_{\mathbf{c}} \left\| \hat{\boldsymbol{\sigma}}_i - \hat{\mathbf{V}}_i\mathbf{c} \right\|_2^2. \quad (4)$$

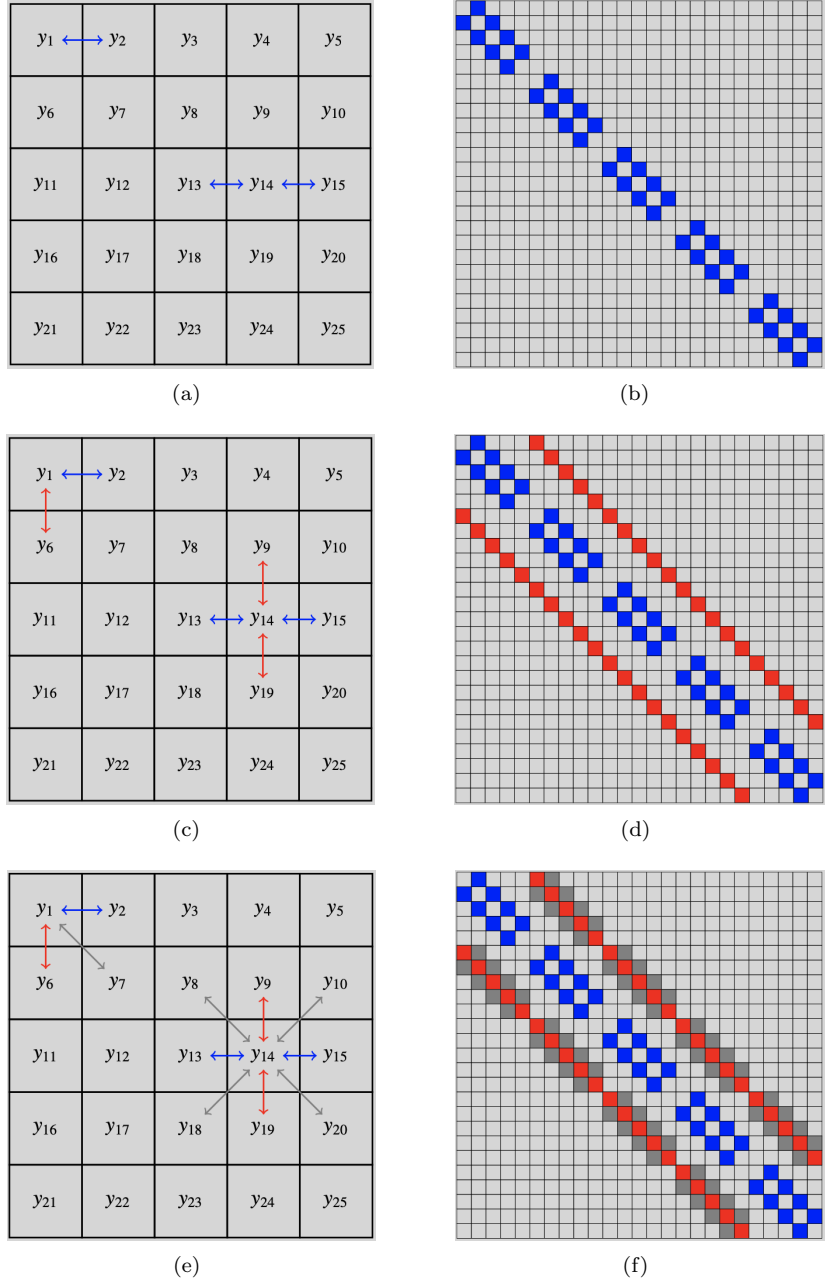


Figure 1: The left figures show (5×5) grids of spatial units with arrows depicting horizontal (blue), vertical (red), and/or diagonal interactions (grey). The right figures illustrate the sparsity pattern associated with these spatial layouts. For example, spatial unit y_1 interacts horizontally with y_2 , vertically with y_6 , and diagonally with y_7 . If these are the only possible interactions for spatial unit y_1 , then only a_{12} , a_{16} , and a_{17} in the first row of \mathbf{A} are possibly nonzero (the interactions for y_{14} are indicated as well). The right figures show the implied corresponding sparsity pattern for all spatial units.

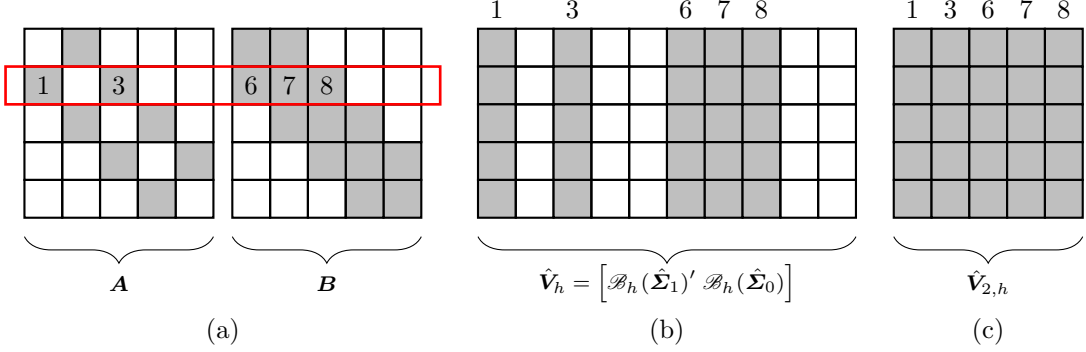


Figure 2: A visualization on the construction of $\hat{\mathbf{V}}_{2,h}$ for $N = 5$. **(a)** If $h = 1$, then grey elements in \mathbf{A} and \mathbf{B} are (potentially) nonzero whereas white elements are zero by construction. Enumerating along the second row, the active elements are in the set $\{1, 3, 6, 7, 8\}$. **(b)** We select the columns from $\hat{\mathbf{V}}_h$ corresponding to the active set. **(c)** The matrix $\hat{\mathbf{V}}_{2,h}$ is the submatrix of $\hat{\mathbf{V}}_h$ with only active columns.

We will adjust this objective function in three ways. First, we define our estimator in terms of banded estimated covariance matrices, which allows us to exploit the results in Theorem 1. Second, our group penalty penalizes parameters across equations so we can no longer estimate the parameters equation-by-equations. We therefore define $\hat{\boldsymbol{\sigma}}_h = \text{vec}(\mathcal{B}_h(\hat{\boldsymbol{\Sigma}}_1)')$ and $\hat{\mathbf{V}}_h^{(d)} = \text{diag}(\hat{\mathbf{V}}_{1,h}, \dots, \hat{\mathbf{V}}_{N,h})$, with $\hat{\mathbf{V}}_{i,h}$ being constructed similarly to \mathbf{V}_i (see Figure 2 for an illustration).³ In this notation, the expression $\|\hat{\boldsymbol{\sigma}}_h - \hat{\mathbf{V}}_h^{(d)} \mathbf{c}\|_2^2$ defines the joint objective function that sums the individual contributions in (4) over all equations. Finally, we construct the penalty function. We define an index set that partitions the vector \mathbf{c} into sub-vectors, denoted $\{\mathbf{c}_g\}$, that contain the non-zero diagonals of \mathbf{A} and \mathbf{B} that are admissible under Assumption 3 as

$$\begin{aligned} \mathcal{G}_A &:= \{g \subset \mathbb{N} : \mathbf{c}_g = \mathcal{D}_A(k), k \in \{1, \dots, \lfloor N/4 \rfloor\}\}, \\ \mathcal{G}_B &:= \{g \subset \mathbb{N} : \mathbf{c}_g = \mathcal{D}_B(k), k \in \{0, \dots, \lfloor N/4 \rfloor\}\}, \end{aligned} \quad (5)$$

respectively, and let $\mathcal{G} = \mathcal{G}_A \cup \mathcal{G}_B$. Based on this notation, we define our objective function as

$$\mathcal{L}_\alpha(\mathbf{c}; \lambda) = \left\| \hat{\boldsymbol{\sigma}}_h - \hat{\mathbf{V}}_h^{(d)} \mathbf{c} \right\|_2^2 + \lambda \underbrace{\left((1 - \alpha) \sum_{g \in \mathcal{G}} \sqrt{|g|} \|\mathbf{c}_g\|_2 + \alpha \|\mathbf{c}\|_1 \right)}_{=: P_\alpha(\mathbf{c})} = \left\| \hat{\boldsymbol{\sigma}}_h - \hat{\mathbf{V}}_h^{(d)} \mathbf{c} \right\|_2^2 + \lambda P_\alpha(\mathbf{c}). \quad (6)$$

The spatial lasso-type shrinkage estimator, abbreviated SPLASH(α, λ) or SPLASH in short, is defined as the minimizer of (6), i.e. $\hat{\mathbf{c}} = \arg \min_{\mathbf{c}} \mathcal{L}_\alpha(\mathbf{c}; \lambda)$. The importance of the penalty function $P_\alpha(\mathbf{c})$ is governed by the penalty parameter λ and a second hyperparameter α balances group-structured sparsity versus individual sparsity. At the extremities of $\alpha \in [0, 1]$ we find the group lasso ($\alpha = 0$) and the lasso ($\alpha = 1$). Intermediate values of α will shrink both groups of diagonal coefficients in \mathbf{A} and \mathbf{B} and individual parameters. The SPLASH solution promotes completely

³In general, all quantities derived from the autocovariance matrices come in three versions: (1) the population quantity, (2) the estimated counterpart without banding denoted with an additional “hat”, and (3) the estimated counterpart with banding featuring both a “hat” and the subscript h .

sparse diagonals and sparse elements within nonzero diagonals, and thus shrinks towards sparsity patterns of the type displayed in Figure 1(b). As the structure of our estimator is similar to that of the sparse group lasso (SGL), efficient algorithms are available to compute its solution (see, e.g. Simon et al., 2013).⁴

3.2 Theoretical Properties of the SPLASH(α, λ) Estimator

In this section we derive the theoretical properties of the SPLASH estimator. First, however, we require an additional assumption on the DGP in order to ensure that \mathbf{A} and \mathbf{B} in (1) are uniquely identified. To this end, we leverage the bandedness assumption in Assumption 3, which enables unique identification of \mathbf{A} and \mathbf{B} via a straightforward full-rank condition on sub-matrices of the autocovariance matrices that appear in the generalized Yule-Walker equations:

Assumption 4 (Restricted minimum eigenvalue). Assume that

$$\phi_{\min}(\mathbf{x}) := \min_{\mathbf{x} \in \mathbb{R}^{2N} : \mathcal{M}(\mathbf{x}) \leq N} \frac{\|\mathbf{V}\mathbf{x}\|_2}{\|\mathbf{x}\|_2} \geq \phi_0.$$

Essentially, Assumption 4 states that every sub-matrix containing N columns from \mathbf{V} has full column-rank and a minimum singular value bounded away from zero. Related assumptions appear in Bickel et al. (2009, Section 4), who refer to $\phi_{\min}(\mathbf{x})$ as a *restricted eigenvalue* and use this quantity to construct sufficient conditions for their restricted eigenvalue assumptions. Assumption 4 fits our framework particularly well, as the assumed maximum bandwidth of the matrices \mathbf{A} and \mathbf{B} in Assumption 3 imply that the diagonal blocks of the matrix $\mathbf{V}^{(d)}$ never contain more than N unique columns of \mathbf{V} . Using this property, we show in Lemma 1 in Appendix A that the SGL compatibility condition is implied by Assumption 4.

Equipped with Assumption 4, we are now able to derive the following finite-sample performance bounds on the prediction and estimation error of SPLASH.

Theorem 2. *Under Assumptions 1-4, it holds that*

$$\left\| \hat{\mathbf{V}}_h^{(d)}(\hat{\mathbf{c}} - \mathbf{c}) \right\|_2^2 + \lambda \left((1 - \alpha) \sum_{g \in \mathcal{G}} \sqrt{|g|} \|\hat{\mathbf{c}}_g - \mathbf{c}_g\|_2 + \alpha \|\hat{\mathbf{c}} - \mathbf{c}\|_1 \right) \leq \frac{64\bar{\omega}_\alpha^2 \lambda^2}{\phi_0^2}$$

with a probability of at least

(a) $1 - 10\mathcal{P}_1(f(\lambda, \phi_0), N, T)$ when Assumption 2(b1) (polynomial tail decay) is valid, or

(b) $1 - 10\mathcal{P}_2(f(\lambda, \phi_0), N, T)$ when Assumption 2(b2) (exponential tail decay) is valid,

where $\mathcal{P}_1(x, N, T)$ and $\mathcal{P}_2(x, N, T)$ are defined in Theorem 1 and $f(\lambda, \phi_0) = \min\left(\frac{\lambda^{1/2}}{24}, \frac{\lambda}{96C_v}, \frac{\phi_0}{12}\right)$.

Theorem 2 contains a finite-sample performance bound for the prediction and estimation error for the SPLASH(α, λ) estimator. The result demonstrates that both errors are increasing in $\bar{\omega}_\alpha$, which in turn is increasing in the bandwidths k_0 and l_0 and the group sizes when $\alpha < 1$ and increasing in the number of relevant interactions $|S|$ when $\alpha > 0$. Furthermore, the prediction and

⁴An R/C++ implementation of the SPLASH estimator based on this algorithm is available on <https://sites.google.com/view/etiennewijler/code>.

estimation error increase along with the imposed amount of penalization λ . While this seems to suggest minimizing the amount of penalization to obtain better performance bounds, we emphasize that the effect of regularization in Theorem 2 is two-fold: increasing the regularization (λ) worsens the performance bound, but increases the probability of the set on which the performance bound holds. Intuitively, the imposed shrinkage induces finite-sample bias in the estimates which worsen the prediction and estimation accuracy. At the same time, however, shrinkage reduces sensitivity to noise, such that performance guarantees can be provided with more certainty.

The aforementioned interactions can be intuitively demonstrated by means of an asymptotic analysis. Accordingly, based on Theorem 2, we derive the conditions for convergence of the prediction and estimation errors, as well as their convergence rates, in the following corollary.

Corollary 1. *Let $\lambda \in O(T^{-q_\lambda})$, $N \in O(T^{q_N})$, $|\mathcal{G}_S| \in O(T^{q_g})$, $|S| \in O(T^{q_s})$, $k_0, l_0 \in O(T^{q_k})$, where q_λ, q_N, q_s , and q_k are fixed and positive constants. Maintain Assumptions 1-4 and assume that either (i) $q_\lambda < -\frac{2q_N}{d} - q_k + \frac{\delta(d-1)}{2d}$ for some $0 < \delta < 1$ and Assumption 2(b1) holds, or (ii) $q_\lambda < \frac{1}{2} - q_k$ and Assumption 2(b2) holds. Then,*

$$(a) \left\| \hat{\mathbf{V}}_h^{(d)} (\hat{\mathbf{c}} - \mathbf{c}) \right\|_2^2 = O_p \left((1 - \alpha) T^{2q_g + q_N - 2q_\lambda} + \alpha T^{q_s - 2q_\lambda} \right),$$

$$(b) (1 - \alpha) \sum_{g \in \mathcal{G}} \sqrt{|g|} \|\hat{\mathbf{c}}_g - \mathbf{c}_g\|_2 + \alpha \|\hat{\mathbf{c}} - \mathbf{c}\|_1 = O_p \left((1 - \alpha) T^{2q_g + q_N - q_\lambda} + \alpha T^{q_s - q_\lambda} \right).$$

Corollary 1 provides detailed insights into the determinants of the convergence rate. In particular, the result confirms that the convergence rate decreases in the bandwidths k_0 and l_0 , the number of spatial units N , the number of interactions $|S|$ and the degree of penalization λ .⁵ To ensure that the set on which the performance bound in Theorem 2 holds occurs with probability converging to one, conditions (i) and (ii) impose that the degree of penalization does not decay too fast. The optimal convergence rate is obtained by choosing q_λ as large as possible without violating these conditions. Several examples are provided in Remark 2.

Remark 2. Several insightful cases can be examined based on Corollary 1. For the sake of brevity, we consider the estimation error, as measured by $P_\alpha(\hat{\mathbf{c}} - \mathbf{c})$, for the case in which the errors possess at least d finite moments (Assumption 2(b1)) in some special cases. First, in the absence of within-group shrinkage (i.e. $\alpha = 0$), Corollary 1 demonstrates that $P_0(\hat{\mathbf{c}} - \mathbf{c}) = O_p(T^{q_N - q_\lambda})$, with $q_\lambda < \frac{1}{2} - \frac{2q_N}{d} - \frac{1}{2d}$ by choosing δ arbitrarily close to 1. Hence, the estimator converges almost at the rate $\frac{T^{1/2 - 1/2d}}{N^{1 + 2/d} |\mathcal{G}_S|}$. For fixed N and large d , this would indeed be close to the optimal \sqrt{T} convergence familiar from the fixed-dimensional case without regularization. Alternatively, when the shrinkage is imposed at the individual interaction level only ($\alpha = 1$), then $P_1(\hat{\mathbf{c}} - \mathbf{c}) = O_p(T^{q_s - q_\lambda})$ such that the estimation error converges almost at the rate $\frac{T^{1/2 - 1/2d}}{|S| N^{2/d}}$, instead.

4 Simulations

4.1 Simulation setting

In this section, we explore the finite sample performance of our estimator by Monte Carlo simulation. The data generating process underlying the simulations is the spatio-temporal VAR in (1). We study $T \in \{500, 1000, 2000\}$ and draw all errors ϵ_{it} independently and $N(0, 1)$ distributed. The matrices

⁵Recall that $\lambda \in O(T^{-q_\lambda})$, such that a higher q_λ implies a faster decay of the penalty term.

\mathbf{A} and \mathbf{B} and the cross-sectional dimension N are specified in the two designs below. All simulation results are based on $N_{sim} = 500$ Monte Carlo replications.

Design A (Banded specification): We revisit simulation Case 1 in Gao et al. (2019). The matrices \mathbf{A} and \mathbf{B} are banded with a bandwidth of $k_0 = 3$. Specifically, the elements in the matrices $(\mathbf{A})_{i,j=1}^N$ and $(\mathbf{B})_{i,j}^N$ are generated according to the following two steps:

Step 1: If $|i - j| = k_0$, then a_{ij} and b_{ij} are drawn independently from a uniform distributions on the two points $\{-2, 2\}$. All remaining elements within the bandwidth are drawn from the mixture distribution $\omega I_{\{0\}} + (1 - \omega)N(0, 1)$ with $\mathbb{P}(\omega = 1) = 0.4$ and $\mathbb{P}(\omega = 0) = 0.6$.

Step 2: Rescale the matrices \mathbf{A} and \mathbf{B} from Step 1 to $\eta_1 \times \mathbf{A} / \|\mathbf{A}\|_2$ and $\eta_2 \times \mathbf{B} / \|\mathbf{B}\|_2$, where η_1 and η_2 are drawn independently from $U[0.4, 0.8]$.⁶

We vary the cross-sectional dimension over $N \in \{25, 50\}$.

Design B (Spatial grid with neighbor interactions): As in Figure 1, we consider an $(m \times m)$ grid of spatial units. For $m = 5$ ($m = 7$), this results in a cross-sectional dimension of $N = 25$ ($N = 49$). The matrix \mathbf{A} contains interactions between first horizontal and first vertical neighbours while all other coefficients are zero. The magnitude of these nonzero interactions are 0.2. For $m = 5$ ($m = 7$), the temporal matrix \mathbf{B} is a diagonal matrix with elements 0.25 (0.23) on the diagonal. The reduced form VAR matrix $\mathbf{C} = (\mathbf{I}_N - \mathbf{A})^{-1}\mathbf{B}$ has a maximum eigenvalue of 0.814 (0.882).

For each design, we report simulation results for three sets of estimators. The first set includes the estimators developed in this paper: (1) the SPLASH(0, λ) estimator promotes non-sparse groups only, (2) the SPLASH(1, λ) encourages unstructured sparsity, and (3) the SPLASH(α , λ) balances group formation and sparse solutions by selecting α in a data-driven way. In congruence with Theorems 1 and 2, we rely on banded autocovariance matrices $\mathcal{B}_h(\hat{\Sigma}_0)$ and $\mathcal{B}_h(\hat{\Sigma}_1)$. The bandwidth choice is determined by the bootstrap procedure described in Guo et al. (2016, p. 7). Second, we include two unpenalized estimators in the spirit of Gao et al. (2019). The estimator GMWY(k_0) implements generalized Yule-Walker estimation for banded \mathbf{A} and \mathbf{B} with the true bandwidth k_0 . GMWY(c_S) is even more informed about the data generating process and estimates true nonzero coefficients only. To allow for easy comparison with the simulation results by the aforementioned authors, we implement these GMWY estimators without banding the covariance matrix estimators $\hat{\Sigma}_0 = \frac{1}{T} \sum_{t=2}^T \mathbf{y}_t \mathbf{y}'_t$ and $\hat{\Sigma}_1 = \frac{1}{T} \sum_{t=2}^T \mathbf{y}_t \mathbf{y}'_{t-1}$.⁷ Note that GMWY(k_0) and GMWY(c_S) are infeasible in practice and are thus given a comparative advantage.⁸ The third set contains the L_1 -penalized reduced form VAR(1) estimator (abbreviated PVAR) only. That is, we

⁶This rescaling does not necessarily imply $\|(\mathbf{I}_N - \mathbf{A})^{-1}\mathbf{B}\|_2 < 1$ (stability). During the simulations we redraw the matrices \mathbf{A} and \mathbf{B} whenever $\|(\mathbf{I}_N - \mathbf{A})^{-1}\mathbf{B}\|_2 > 0.95$.

⁷In unreported simulation results, that are available upon request, we find that the results are insensitive to this choice.

⁸A (consistent) ratio-based estimator for k_0 is described on page 214 of Gao et al. (2019). A feasible two-step estimation procedures is: (1) estimate k_0 using the ratio-based estimator (i.e. compute \hat{k}), and (2) estimate the spatio-temporal VAR assuming \mathbf{A} and \mathbf{B} have bandwidth \hat{k} . As in Gao et al. (2019), we also observed a (small) tendency to overestimate k_0 . In high-dimensional settings, this causes highly volatile parameter estimates and performance issues. We thus decided to provide either k_0 or the true sparsity structure. Gao et al. (2019) also propose estimators that use multiple Yule-Walker equations or pre-select the estimating equations that are most informative about the parameters. In their simulation section, see Gao et al. (2019, p. 219), they state that these estimators do not provide clear benefits. As such, we decided to not include these estimators in our simulation study.

consider the reduced form VAR(1) specification $\mathbf{y}_t = \mathbf{C}\mathbf{y}_{t-1} + \mathbf{u}_t$ and estimate \mathbf{C} by minimizing $\mathcal{L}_{pvar}(\mathbf{C}) = \sum_{t=2}^T \|\mathbf{y}_t - \mathbf{C}\mathbf{y}_{t-1}\|_2^2 + \lambda \sum_{i,j=1}^N |c_{ij}|$. This estimator is well-researched in the literature (see, e.g. Kock and Callot, 2015; Gelper et al., 2016; Masini et al., 2019), albeit in different settings. It will serve as a competitive benchmark for the forecasting performance of our proposed estimation procedure.

The forecasting performance of each estimator is assessed by the relative mean-squared forecast error (RMSFE). Using a superscript j to index the Monte Carlo replications, the RMSFE is calculated as

$$\text{RMSFE} = \frac{\sum_{j=1}^{N_{sim}} \left\| \mathbf{y}_{T+1}^j - \hat{\mathbf{C}}^j \mathbf{y}_T^j \right\|_2^2}{\sum_{j=1}^{N_{sim}} \left\| \mathbf{y}_{T+1}^j - \mathbf{C} \mathbf{y}_T^j \right\|_2^2}.$$

As the SPLASH and GMWY procedures estimate \mathbf{A} and \mathbf{B} , we can also compare the estimation accuracy. Using the superscript j as before, the *Estimation Error (EE)* of the coefficient matrices are:

$$\text{EE}_A = \frac{1}{N_{sim}} \sum_{j=1}^{N_{sim}} \left\| \hat{\mathbf{A}}^j - \mathbf{A} \right\|_2, \text{ and } \text{EE}_B = \frac{1}{N_{sim}} \sum_{j=1}^{N_{sim}} \left\| \hat{\mathbf{B}}^j - \mathbf{B} \right\|_2. \quad (7)$$

Finally, the hyperparameter, λ (and also α for the SPLASH(α, λ) estimator), for the SPLASH and PVAR estimators are selected based on time series cross-validation. The grid for λ consists of 20 evenly spaced values on a logarithmic scale. The maximum value for λ is the smallest value that gives the zero solution and the minimum value is set to 10^{-4} times the maximum. For α , the admissible values are $\alpha \in \{0, 0.25, 0.5, 0.75, 1\}$. For each choice of hyperparameters, we estimate the model on the first 80% of the data and evaluate the out-of-sample fit on the last 20% of the data. The hyperparameters with the lowest out-of-sample model error are chosen.

4.2 Simulation results

The results for Design A are reported in Table 1. First, we consider the predictive performance. Across all specifications, the penalized VAR estimator is outperformed by all other estimators, indicating that direct estimation of the contemporaneous spatial interactions can deliver forecast improvements over regularized reduced form estimation. A plausible explanation for this finding is that the sparsity patterns in the spatial representation are less prevalent, and thus more difficult to exploit, in the reduced form representation. Overall, and in line with expectations, the best predictor is the infeasible GMWY(c_s) estimator, which requires knowledge of the exact sparsity pattern. Alternatively, the best feasible estimators are SPLASH(0, λ) and SPLASH(α, λ), who obtain nearly equivalent performance, since the cross-validation approach decides on $\alpha = 0$ in the overwhelming majority of simulation trials. Moreover, for smaller samples ($T = 500$), the SPLASH estimators obtain a forecast accuracy is notable higher than that obtained by GMWY(k_0). However, as the latter improves rapidly in T , the performance gains of SPLASH are less notable for $T = 1000$ and absent for $T = 2000$.

Next, we explore the estimation accuracy. For SPLASH(0, λ) and SPLASH(α, λ), the estimation error decreases in T . This is to be expected since an increasing sample size will result in more accurate estimates for $\boldsymbol{\Sigma}_0$ and $\boldsymbol{\Sigma}_1$ and thus (through the Yule-Walker equations) better parameter estimates and forecasts. Somewhat counter-intuitively, however, SPLASH(1, λ) seems to attain worse estimation accuracy on larger samples. Since the penalty is chosen by cross-validation,

Table 1: Simulation results for Design A (Banded specification).

N	T	SPLASH(0, λ)	SPLASH(α , λ)	SPLASH(1, λ)	GMWY(k_0)	GMWY(c_S)	PVAR
Relative Mean-Squared Forecast Error (RMSFE)							
25	500	1.013	1.014	1.023	1.039	1.018	1.106
	1,000	1.010	1.011	1.019	1.016	1.008	1.108
	2,000	1.004	1.005	1.010	1.004	1.002	1.122
50	500	1.019	1.019	1.035	1.033	1.018	1.108
	1,000	1.010	1.010	1.020	1.018	1.010	1.101
	2,000	1.009	1.009	1.013	1.008	1.006	1.101
100	500	1.022	1.023	1.040	1.034	1.021	1.115
	1,000	1.014	1.014	1.025	1.018	1.013	1.106
	2,000	1.009	1.009	1.015	1.010	1.007	1.103
Estimation Error in A (EEA)							
25	500	0.549	0.552	0.836	1.208	0.689	
	1,000	0.527	0.527	0.854	1.095	0.588	
	2,000	0.489	0.491	0.854	1.018	0.491	
50	500	0.558	0.557	0.954	0.899	0.634	
	1,000	0.529	0.529	0.968	0.783	0.537	
	2,000	0.506	0.504	1.010	0.702	0.450	
100	500	0.555	0.554	0.928	0.764	0.593	
	1,000	0.521	0.519	0.917	0.689	0.519	
	2,000	0.502	0.499	0.976	0.598	0.440	
Estimation Error in B (EEB)							
25	500	0.282	0.284	0.386	0.417	0.244	
	1,000	0.243	0.244	0.356	0.342	0.187	
	2,000	0.207	0.208	0.330	0.295	0.146	
50	500	0.305	0.306	0.436	0.368	0.250	
	1,000	0.257	0.257	0.394	0.277	0.186	
	2,000	0.222	0.220	0.380	0.218	0.139	
100	500	0.323	0.323	0.449	0.359	0.263	
	1,000	0.273	0.272	0.404	0.267	0.196	
	2,000	0.234	0.231	0.383	0.207	0.147	

Note: The relative mean-squared forecast error (RMSFE) and estimation errors (EE_A and EE_B) of design A. Lower numbers indicate better performance. As PVAR estimates a reduced form VAR, there are no model errors for **A** and **B** to report for this method.

Table 2: Simulation results for Design B (Spatial grid with neighbor interactions).

N	T	SPLASH(0, λ)	SPLASH(α , λ)	SPLASH(1, λ)	GMWY(k_0)	GMWY(c_S)	PVAR
Relative Mean-Squared Forecast Error (RMSFE)							
25	500	1.011	1.025	1.046	1,573.644	1.011	1.109
	1,000	1.004	1.016	1.032	23.176	1.004	1.068
	2,000	1.008	1.025	1.019	7.441	1.004	1.043
100	500	1.023	1.029	1.086	131.346	1.015	1.168
	1,000	1.011	1.023	1.037	37.423	1.011	1.116
	2,000	1.007	1.017	1.015	1.170	1.004	1.070
Estimation Error in A (EEA)							
25	500	0.322	0.351	0.832	4.187	0.435	
	1,000	0.277	0.327	0.718	3.968	0.313	
	2,000	0.232	0.318	0.648	3.773	0.224	
100	500	0.351	0.349	1.066	2.078	0.549	
	1,000	0.328	0.339	0.913	2.030	0.473	
	2,000	0.291	0.316	0.769	2.010	0.388	
Estimation Error in B							
25	500	0.102	0.141	0.338	1.269	0.137	
	1,000	0.087	0.137	0.298	1.098	0.095	
	2,000	0.072	0.134	0.248	0.966	0.069	
100	500	0.105	0.114	0.361	0.906	0.218	
	1,000	0.095	0.123	0.324	0.687	0.160	
	2,000	0.080	0.121	0.282	0.553	0.120	

Note: The relative mean-squared forecast error (RMSFE) and estimation errors (EE_A and EE_B) of design B. Lower numbers indicate better performance. As PVAR estimates a reduced form VAR, there are no model errors for \mathbf{A} and \mathbf{B} to report for this method.

which solely focuses on out-of-sample predictive performance, we conjecture that the most accurate estimates may not always be the one that delivers the most accurate predictive performance within a given sample. Regarding the performance differentials across methods, the implied performance ranking largely coincides with the ranking based on the relative mean-squared forecast error. SPLASH(0, λ) and SPLASH(α , λ) obtain the lowest estimation error, narrowly followed by the infeasible GMWY(c_S). The GMWY(k_0) performs notably worse than SPLASH in small samples, but closes the gap somewhat when T increases.

Simulation results for Design B are shown in Table 2. The high RMSFEs for GMWY(k_0) in comparison to all competing models are most striking. However, do recall that this approach cannot exploit any sparsity as present in the sparse representations for \mathbf{A} and \mathbf{B} in this design. For instance, looking at Figure 3(a) we see that the entries a_{ij} of \mathbf{A} with $|i - j| \leq 5$ contain 165 zeros and 80 nonzeros for $N = 25$. The matrix \mathbf{A} within the correct bandwidth is thus 51.52% sparse. Any unpenalized approach is likely overparameterized which explains the bad forecasting performance and high estimation errors that is especially pronounced in small samples. The other results tell the same story as in Design A; SPLASH(0, λ) and SPLASH(α , λ) are performing very close to the optimal, though infeasible, GMWY(c_S) estimator, and forecast notably better than the PVAR. SPLASH(1, λ) ranks in-between these approaches, as it benefits from the direct estimation of spatial interactions, but does so less efficiently by not taking into account the diagonally structured form of sparsity.

A small visual analysis provides further evidence on the good estimation accuracy obtained by $\text{SPLASH}(\alpha, \lambda)$. That is, we can visualize the capability of recovering the correct sparsity pattern by displaying the absolute value of the coefficients as averaged across all N_{sim} simulation runs. Figure 3 illustrates the similarity between the true matrix \mathbf{A} and the average magnitude of the estimated coefficients.

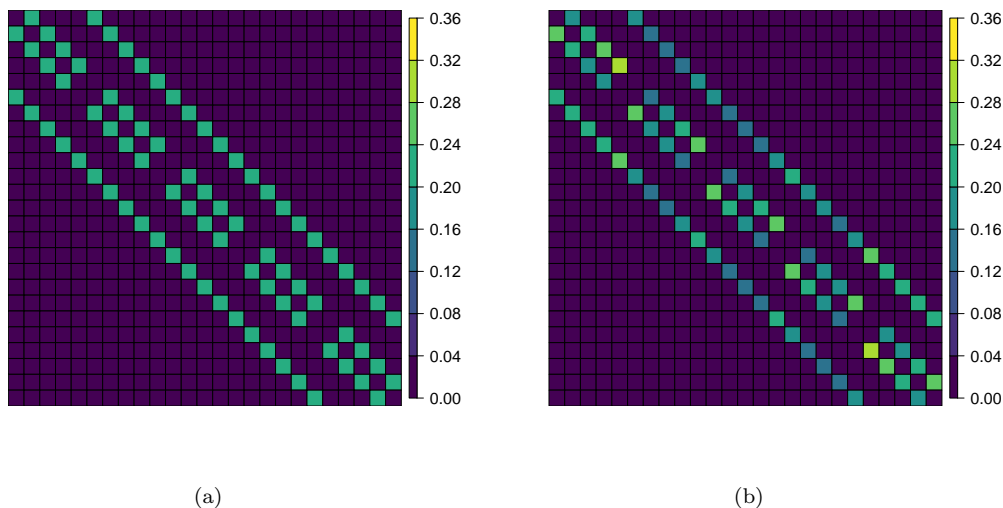


Figure 3: Visualizations of the true and estimated spatial weight matrix \mathbf{A} for Design B. (a) The true spatial weight matrix \mathbf{A} implied by the (5×5) spatial grid design (Design B with $m = 5$). (b) The average absolute values of the entries in $\hat{\mathbf{A}}$ as computed by $\text{SPLASH}(\alpha, \lambda)$ for $N = 25$ and $T = 1000$. That is, the $(i, j)^{\text{th}}$ entry in the matrix on the right equals $\frac{1}{N_{sim}} \sum_{k=1}^{N_{sim}} |\hat{a}_{ij}^k|$ with \hat{a}_{ij}^k being the estimated $(i, j)^{\text{th}}$ entry of \mathbf{A} in the k^{th} Monte Carlo replication.

Remark 3. In elaborate, though unreported, visual analysis, we find that most zero diagonals are actually not estimated as exactly zero by the (sparse) group lasso. When tuning the penalty parameter by the BIC criterion, in which the number of estimated non-zeros is used as a proxy for the degrees of freedom, the true zero diagonals are typically estimated as exactly zeros. However, the increased amount of regularization that is required to effectuate this has a negative impact on the forecast performance.

5 Empirical Application

We examine the empirical performance of the SPLASH estimator when predicting daily NO_2 concentrations in (Greater) London. The data is publicly available via the Copernicus Open Access Hub and we consider the time span from 1 August 2018 to 18 October 2020.⁹ The original NO_2 concentrations are reported in mol/m^2 but we convert to mol/cm^2 to avoid numerical instabilities

⁹See <http://www.tropomi.eu/> for more info on the TROPOMI data products, and use <https://scihub.copernicus.eu/> to access the database.

caused by the use of small-scale numbers. The far majority of measurements are captured sometime between 11:00 and 14:00 UTC. The area of interest is divided into a (5×9) grid, implying that longitudes and latitudes increment by approximately 0.2 from cell to cell. All available NO_2 measurements are averaged within each cell and within the same day. The resulting data set has 0.8% missing observations. These missing values are imputed using the **Multivariate Time Series Data Imputation (mtsdi)** R package.¹⁰

A rolling-window approach is used to assess the predictive power of the SPLASH estimator. Each window contains 80% of the data, or 641 days, such that a total of 160 one-step ahead forecasts can be produced. For each window, we proceed along the following four steps: (i) de-mean the data, (ii) determine the hyperparameters and estimate each model, (iii) produce a forecast for the de-meaned data, and (iv) add the means back to the forecast. In addition to the estimators described in the simulation section (Section 4, see page 11), we add another forecast: the window’s mean. This new forecast is abbreviated CONST and all other forecasts follow the notational conventions from the simulation section. Similarly, all tuning parameters are chosen via the time-series cross-validation procedure outlined in Section 4. The spatial grid contains $N = 5 \times 9 = 45$ spatial units, such that the $\text{SPLASH}(\alpha, \lambda)$ models contain $2N^2 - N = 4,005$ parameters. For the purpose of identifiability, we band the spatial matrix \mathbf{A} and autoregressive matrix \mathbf{B} such that $a_{ij} = b_{ij} = 0$ for $|i - j| > \lfloor N/4 \rfloor = 11$. By ordering the spatial units vertically, this banding puts no restrictions on the degree of vertical interaction but allows no more than second-order interaction between horizontal neighbours (see Figure 5 in Appendix C.1 for details).

The forecast performance is measured along three metrics and always relative to the L_1 -penalized reduced form VAR(1) (PVAR) benchmark. That is, we report: (i) the number of spatial units that are predicted more accurately than the PVAR method ($\#$ wins), (ii) the number of spatial units that are predicted *significantly* more accurately based on a Diebold-Mariano test at the the 5% significance level ($\#$ sign.), and (iii) the average loss relative to the penalized VAR over all spatial units. These three metrics are calculated based on two loss functions for the forecast errors, namely the mean squared forecast error (MSFE) and the mean absolute forecast error (MAFE). We report the MAFE because the NO_2 column densities display several abrupt spikes which may carry to much weight when relying on a squared loss function. The results are reported in Table 3.

We first look at the mean squared forecast errors (MSFEs). The window-mean forecast (CONST) clearly does not improve the benchmark PVAR forecast for any spatial unit. However, this forecast still attains a RMSFE of 1.185, potentially indicating a low predictability of NO_2 column densities. The GMWY approach obtains the worst forecast performance, possibly because relatively large bandwidths are needed to allow for second-order horizontal interaction, thereby paralleling our findings from the simulations. $\text{SPLASH}(0, \lambda)$ improves upon the benchmark for all 45 spatial units, 42 of which are found to be significant by a Diebold-Mariano test (based on the absolute forecast errors). Allowing for sparsity within groups does not deliver additional forecast improvements as $\text{SPLASH}(\alpha, \lambda)$ attains a slightly worse forecast performance than the SPLASH specification with group penalty only ($\alpha = 0$). Completely omitting regularization at the group level further deteriorate the forecast performance, with $\text{SPLASH}(1, \lambda)$ only beating the benchmark for 34 out 45 spatial units, 14 of which are statistically significant. We take this as evidence that the ability to promote diagonally structured sparsity is indeed beneficial in real-life spatial applications.

Next, we focus on the mean absolute forecast error (MAFE). The results are qualitatively similar to those obtained based on the MSFE. In particular, GMWY obtains the worst forecast accuracy for

¹⁰This imputation method is proposed by Junger and Ponce De Leon (2015) to impute missing values in time series for air pollutants. The package is written by the same authors and currently maintained by W. L. Junger.

Table 3: Forecast performance of various methods for NO₂ satellite data on a (5 × 9) grid of observations.

	MSFE			MAFE		
	#wins	#sign. wins	RMSFE	#wins	#sign. wins	RMAFE
CONST	0	0	1.185	0	0	1.139
GMWY	0	0	153.122	0	0	4.851
SPLASH(0,λ)	45	42	0.917	45	43	0.939
SPLASH(α,λ)	44	30	0.941	44	32	0.961
SPLASH(1,λ)	34	14	0.969	36	20	0.975

Note: Number of grid points (out of $N = 45$) with lower prediction errors (#wins) and significantly lower prediction errors (#sign.) compared to the L_1 -penalized reduced form VAR(1) estimator (PVAR). Relative MAFE and MSFE are abbreviated by RMAFE and RMSFE, respectively. Values below (above) 1 indicate superior (inferior) performance compared to PVAR.

GMWY, whereas SPLASH(0,λ) forecasts best. The GMWY method, while still standing out, does not score as poorly anymore based on the RMAFE. We conjecture that the absence of regularization may increase sensitivity to noise, thereby resulting in particularly high squared forecast errors at periods of atypical NO₂ concentrations.

Finally, we illustrate the second key benefit of SPLASH-type estimators: interpretability. Recall that we convoluted satellite images to a (5 × 9) grid of spatial units. To examine the relevant interactions between these spatial units, we provide several visualizations of the spatial weight matrices estimated by the SPLASH(0.5,λ) estimator in Figure 4. First, in panel (a), we visualize the absolute magnitude of the spatial interactions. A clear diagonal pattern emerges, with the two diagonals closest to the principal diagonal and the two outer diagonals containing the largest interactions. These four diagonals correspond to first-order vertical and second-order horizontal interactions, respectively. The additional two diagonals, that are sandwiched in between the former, contain the first-order horizontal interactions between spatial units, which surprisingly seem to be smaller in magnitude. In panel (b), each cell indicates the proportion of rolling windows the corresponding spatial interaction is estimated as being non-zero. It turns out, that these proportions are either one (yellow) or zero (purple), indicating very stable selection across samples. It becomes apparent that in addition to the six diagonals that were clear from panel (a), two additional diagonals are always selected, which contain the first order diagonal interactions between spatial units. To facilitate interpretation of this sparsity pattern, we provide a spatial plot of our region of interest in panel (c), with the spatial grid overlaid. For two pixels on this vertically labelled spatial grid, we visualize the interactions implied by panel (b), namely pixel 1 (left-top) and 23 (center) with the use of arrows whose thickness is determined by the average absolute magnitudes estimated in panel (a). The pattern of spatial interactions that emerges clearly shows the interactions between NO₂ concentrations of neighbouring districts in London. The wider horizontal interactions, as well as the diagonal interactions, may be explainable by the “prevailing winds”, which come from the West or South-West and are the most commonly occurring winds in London. Overall, the intuitive sparsity patterns that arise, in combination with the improvement in forecast performance, are encouraging and provide empirical validation for the use of SPLASH on spatial data, especially when the spatial units follow a natural ordering on a spatial grid.

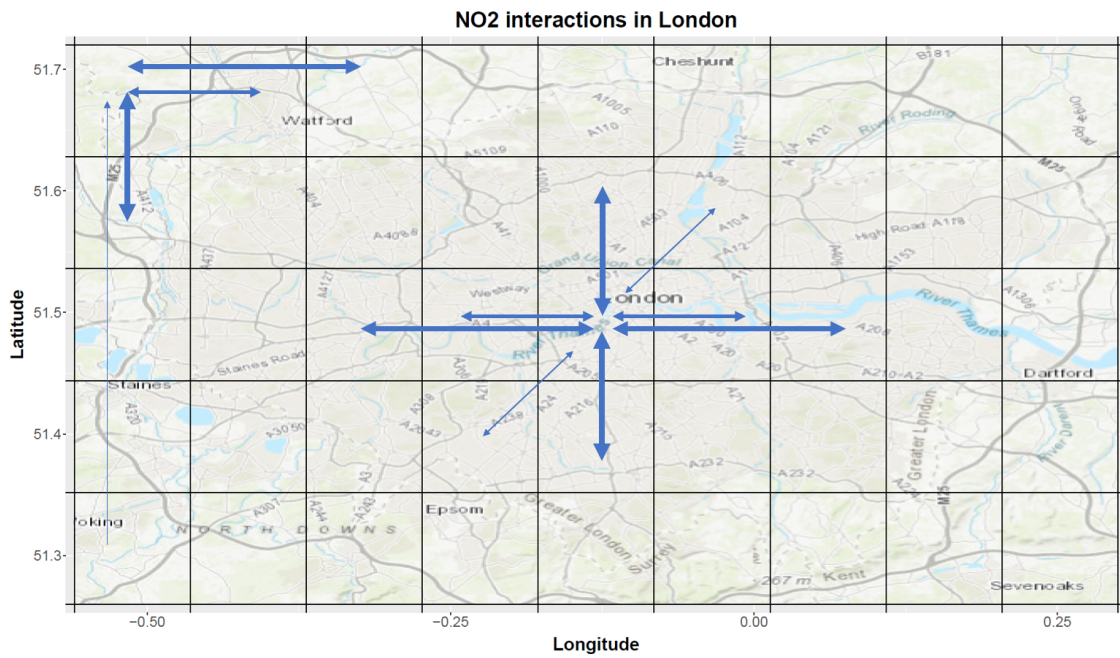
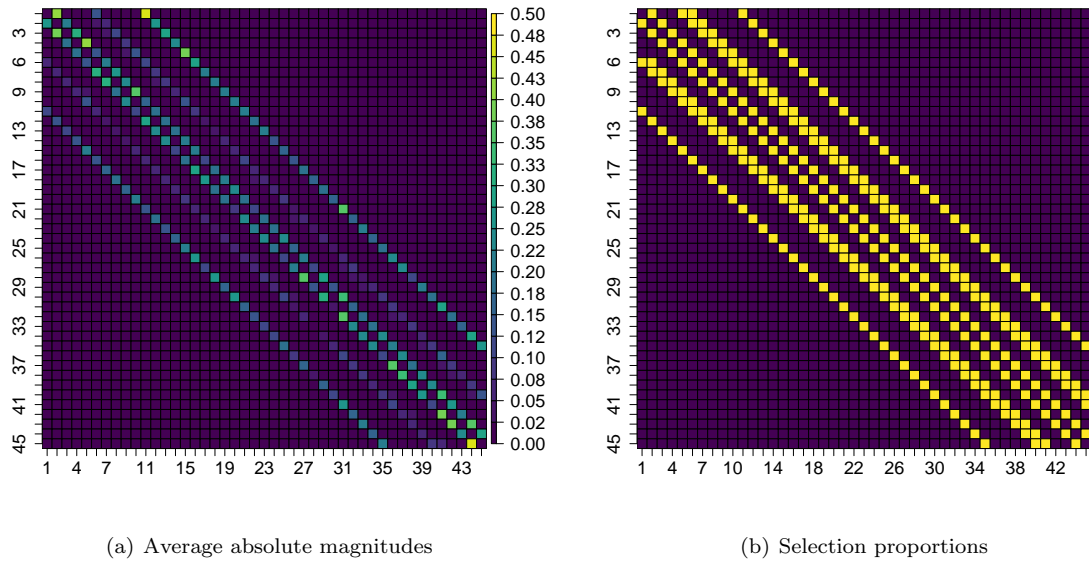


Figure 4: Sparsity patterns for estimates of \mathbf{A} based on rolling window samples.

6 Conclusion

In this paper, we develop the Spatial Lasso-type Shrinkage (SPLASH) estimator, a novel estimation procedure for high-dimensional spatio-temporal models. The SPLASH estimator is designed to promote the recovery of diagonally structured forms of sparsity, which are argued to occur in numerous realistic settings, whilst not imposing said structure a priori. We derive consistency of our estimator in a joint asymptotic framework in which both the number of spatial units and the temporal observations diverge. To solve the identifiability issue, we rely on a relatively non-restrictive assumption that the coefficient matrices in the spatio-temporal model are sufficiently banded. Based on this assumption, we consider banded estimation of high-dimensional spatio-temporal autocovariance matrices, for which we derive novel convergence rates that are likely to be of independent interest. As an application, we use SPLASH to model NO₂ concentrations in London based on satellite data and we find convincing evidence for the presence of spatial interactions between horizontally and vertically neighbouring regions. In addition, our estimator obtains superior forecast accuracy compared to a number of competitive benchmarks, including the recently introduced spatio-temporal estimator by Gao et al. (2019) that formed the inspiration for the development of SPLASH.

7 Acknowledgements

This paper (or earlier versions hereof) has been presented at the seminar of the Quantitative Economics department of Maastricht University, the Econometrics Internal Seminar (EIS) at Erasmus University Rotterdam, and the online Bernoulli-IMS One World Symposium. We gratefully acknowledge comments and feedback from the participants. Suggestions by Stephan Smeekes and Ines Wilms have been particularly helpful so we thank them explicitly. All remaining errors are our own.

References

- Ahrens, A. and Bhattacharjee, A. (2015). Two-step lasso estimation of the spatial weights matrix. *Econometrics*, 3:128–155.
- Bickel, P. J., Ritov, Y., and Tsybakov, A. B. (2009). Simultaneous analysis of lasso and Dantzig selector. *The Annals of Statistics*, 37:1705–1732.
- Brockwell, P. J. and Davis, R. A. (1991). *Time Series: Theory and Methods*. Springer-Verlag, New York, 2nd edition.
- Debarsy, N. and LeSage, J. (2018). Flexible dependence modeling using convex combinations of different types of connectivity structures. *Regional Science and Urban Economics*, 69:48–68.
- Dou, B., Parrell, M. L., and Yao, Q. (2016). Generalized Yule-Walker estimation for spatio-temporal models with unknown diagonal coefficients. *Journal of Econometrics*, 194:369–382.
- Gao, Z., Ma, Y., Wang, H., and Yao, Q. (2019). Banded spatio-temporal autoregressions. *Journal of Econometrics*, 208:211–230.

- Gelper, S., Wilms, I., and Croux, C. (2016). Identifying demand effects in a large network of product categories. *Journal of Retailing*, 92:25–39.
- Guo, S., Wang, Y., and Yao, Q. (2016). High-dimensional and banded vector autoregressions. *Biometrika*, 103:889–903.
- Jing, B.-Y., Shao, Q.-M., and Wang, Q. (2003). Self-normalized Cramér-type large deviations for independent random variables. *Annals of Probability*, 31:2167–2215.
- Junger, W. L. and Ponce De Leon, A. (2015). Imputation of missing data in time series for air pollutants. *Atmospheric Environment*, 102:96–104.
- Kock, A. B. and Callot, L. (2015). Oracle inequalities for high dimensional vector autoregressions. *Journal of Econometrics*, 186:325–344.
- Lam, C. and Souza, P. C. L. (2014). Regularization for spatial panel time series using the adaptive lasso. Working paper, London School of Economics and Political Science.
- Lam, C. and Souza, P. C. L. (2019). Estimation and selection of spatial weight matrix in a spatial lag model. *Journal of Business & Economic Statistics*, 38:1–41.
- Lee, L.-F. (2004). Asymptotic distributions of quasi-maximum likelihood estimators for spatial autoregressive models. *Econometrica*, 72:1899–1925.
- Lee, L.-F. and Yu, J. (2010). Estimation of spatial autoregressive panel data models with fixed effects. *Journal of Econometrics*, 154:165–185.
- Lee, L.-f. and Yu, J. (2014). Efficient GMM estimation of spatial dynamic panel data models with fixed effects. *Journal of Econometrics*, 180:174–197.
- Ma, Y., Guo, S., and Wang, H. (2021). Sparse spatio-temporal autoregressions by profiling and bagging. *Journal of Econometrics*, X:XX–XX.
- Masini, R. P., Medeiros, M. C., and Mendes, E. F. (2019). Regularized estimation of high-dimensional vector autoregressions with weakly dependent innovations. arXiv e-prints 1912.09002, arXiv.
- Simon, N., Friedman, J., Hastie, T., and Tibshirani, R. (2013). A sparse-group lasso. *Journal of Computational and Graphical Statistics*, 22:231–245.
- van der Vaart, A. W. and Wellner, J. A. (1996). *Weak Convergence and Empirical Processes*. Springer.
- Wainwright, M. J. (2019). *High-dimensional Statistics: A Non-asymptotic Viewpoint*. Cambridge University Press.
- Yu, J., de Jong, R., and Lee, L.-f. (2012). Estimation for spatial dynamic panel data with fixed effects: The case of spatial cointegration. *Journal of Econometrics*, 167:16–37.
- Yu, J., de Jong, R. M., and Lee, L.-F. (2008). Quasi-maximum likelihood estimators for spatial dynamic panel data with fixed effects when both n and T are large. *Journal of Econometrics*, 146:118–134.
- Zhang, X. and Yu, J. (2018). Spatial weight matrix selection and model averaging for spatial autoregressive models. *Journal of Econometrics*, 203:1–18.

Appendix A Lemmas

Lemma 1. Define the quantities $N_c = |c|$, $S = \{j : c_j \neq 0\}$, $\mathcal{G}_S = \{g \in \mathcal{G} : \mathbf{c}_g \neq \mathbf{0}\}$, $\mathcal{G}_S^c = \{g \in \mathcal{G} : \mathbf{c}_g = \mathbf{0}\}$, $\bar{\omega}_\alpha = \max \left\{ (1 - \alpha) \sum_{g \in \mathcal{G}_S} \sqrt{|g|}, \alpha \sqrt{|S|} \right\}$ and consider

$$\Delta \in \mathcal{C}_{N_c}(\mathcal{G}, S) := \left\{ \Delta \in \mathbb{R}^{N_c} : P_{\alpha, S^c}(\Delta) \leq 3P_{\alpha, S}(\Delta) \right\},$$

where

$$P_{\alpha, S^c}(\Delta) = (1 - \alpha) \sum_{g \in \mathcal{G}_S^c} \sqrt{|g|} \|\Delta_g\|_2 + \alpha \|\Delta_{S^c}\|_1, \text{ and}$$

$$P_{\alpha, S}(\Delta) = (1 - \alpha) \sum_{g \in \mathcal{G}_S} \sqrt{|g|} \|\Delta_g\|_2 + \alpha \|\Delta_S\|_1.$$

Then, under Assumption 4, it holds that

$$\min_{\Delta \in \mathcal{C}_{N_c}(\mathcal{G}, S)} \frac{\bar{\omega}_\alpha \left\| \mathbf{V}^{(d)} \Delta \right\|_2}{P_{\alpha, S}(\Delta)} \geq \frac{\phi_0}{2}. \quad (8)$$

Proof. First, we show that (8) is bounded from below by $\frac{1}{2}$ times the smallest singular value of $\mathbf{V}^{(d)}$. For $0 \leq \alpha < 1$, it holds that

$$\frac{(1 - \alpha) \sum_{g \in \mathcal{G}_S} \sqrt{|g|} \|\Delta_g\|_2}{\bar{\omega}_\alpha} \leq \frac{\|\Delta\|_2 \sum_{g \in \mathcal{G}_S} \sqrt{|g|}}{\sum_{g \in \mathcal{G}_S} \sqrt{|g|}} = \|\Delta\|_2$$

Alternatively, for $\alpha = 1$, we have $\frac{\alpha \|\Delta_S\|_1}{\bar{\omega}_\alpha} = \frac{\|\Delta_S\|_1}{\sqrt{|S|}} \leq \|\Delta\|_2$. Combining the two previous results yields

$$\frac{P_{\alpha, S}(\Delta)}{\bar{\omega}_\alpha} = \frac{(1 - \alpha) \sum_{g \in \mathcal{G}_S} \sqrt{|g|} \|\Delta_g\|_2 + \alpha \|\Delta_S\|_1}{\bar{\omega}_\alpha} \leq 2 \|\Delta\|_2,$$

for any $0 \leq \alpha \leq 1$.

Next, the result in Lemma 1 follows by noting that $\mathbf{V}^{(d)} = \text{diag}(\mathbf{V}_1, \dots, \mathbf{V}_N)$ is a block-diagonal matrix whose singular values correspond to those of its sub-blocks. Let N_i denote the number of columns of \mathbf{V}_i and note that $N_i < N$ by construction. Then,

$$\begin{aligned} \min_{\Delta \in \mathcal{C}_{N_c}(\mathcal{G}, S)} \frac{\bar{\omega}_\alpha \left\| \mathbf{V}^{(d)} \Delta \right\|_2}{P_{\alpha, S}(\Delta)} &\geq \min_{\Delta \in \mathbb{R}^{N_c}} \frac{\left\| \mathbf{V}^{(d)} \Delta \right\|_2}{2 \|\Delta\|_2} = \min_{1 \leq i \leq N} \min_{\Delta \in \mathbb{R}^{N_i}} \frac{\|\mathbf{V}_i \Delta\|_2}{2 \|\Delta\|_2} \\ &\stackrel{(i)}{\geq} \min_{\Delta \in \mathbb{R}^{2N} : \|\Delta\|_0 \leq N} \frac{\|\mathbf{V} \Delta\|_2}{2 \|\Delta\|_2} \stackrel{(ii)}{\geq} \frac{\phi_0}{2}, \end{aligned}$$

where (i) follows since $N_i < N$ for all $i = 1, \dots, N$ and (ii) holds by Assumption 4. \square

Lemma 2. Define the set $\mathcal{V}(x) := \left\{ \left\| \hat{\mathbf{V}}_h - \mathbf{V} \right\|_2 \leq x \right\}$. Then, under Assumption 4, it holds on $\mathcal{V}(\frac{\phi_0}{4})$ that

$$\min_{\mathbf{x} \in \mathcal{C}_{N_c}(\mathcal{G}, S)} \frac{\bar{\omega}_\alpha \left\| \hat{\mathbf{V}}_h^{(d)} \mathbf{x} \right\|_2}{P_{\alpha, S}(\mathbf{x})} \geq \frac{\phi_0}{4}.$$

Proof. First, recall the construction of $\hat{\mathbf{V}}_h^{(d)} = \text{diag}(\hat{\mathbf{V}}_{1,h}, \dots, \hat{\mathbf{V}}_{N,h})$ with $\hat{\mathbf{V}}_{i,h}$ containing at most $N - 1$ columns of the matrix $\hat{\mathbf{V}}_h = \left(\mathcal{B}_h(\hat{\Sigma}'_1), \mathcal{B}_h(\hat{\Sigma}'_0) \right)$. From the block-diagonal construction, it follows that

$$\left\| \hat{\mathbf{V}}_h^{(d)} - \mathbf{V}^{(d)} \right\|_2 = \max_{1 \leq i \leq N} \left\| \hat{\mathbf{V}}_{i,h} - \mathbf{V}_i \right\|_2 \leq \left\| \hat{\mathbf{V}}_h - \mathbf{V} \right\|_2.$$

Then,

$$\left\| \hat{\mathbf{V}}_h^{(d)} \mathbf{x} \right\|_2 \geq \left\| \mathbf{V}^{(d)} \mathbf{x} \right\|_2 - \left\| \left(\hat{\mathbf{V}}_h^{(d)} - \mathbf{V}^{(d)} \right) \mathbf{x} \right\|_2 \geq \left\| \mathbf{V}^{(d)} \mathbf{x} \right\|_2 - \left\| \hat{\mathbf{V}}_h - \mathbf{V} \right\|_2 \|\mathbf{x}\|_2 \geq \left\| \mathbf{V}^{(d)} \mathbf{x} \right\|_2 - \frac{\phi_0}{2} \|\mathbf{x}\|_2, \quad (9)$$

where the last inequality follows holds on the set $\mathcal{V} \left(\frac{\phi_0}{4} \right)$. Consequently,

$$\min_{\mathbf{x} \in \mathcal{C}_{N_c}(\mathcal{G}, S)} \frac{\omega_\alpha \left\| \hat{\mathbf{V}}_h^{(d)} \mathbf{x} \right\|_2}{P_{\alpha, S}(\Delta)} \stackrel{(i)}{\geq} \min_{\mathbf{x} \in \mathbb{R}^{N_c}} \frac{\left\| \hat{\mathbf{V}}_h^{(d)} \mathbf{x} \right\|_2}{2 \|\mathbf{x}\|_2} \stackrel{(ii)}{\geq} \min_{\mathbf{x} \in \mathbb{R}^{N_c}} \frac{\left\| \mathbf{V}^{(d)} \mathbf{x} \right\|_2}{2 \|\mathbf{x}\|_2} - \frac{\phi_0}{4} \stackrel{(iii)}{\geq} \frac{\phi_0}{4},$$

where (i) follows from the proof of Lemma 1, (ii) by (9) and (iii) from Lemma 1. \square

Lemma 3. *Let Assumptions 1 and 2 hold. Moreover, let $i \in \{1, 2, \dots, N\}$ be an arbitrary index and let x be non-negative.*

(a) *Under polynomial tail decay of the innovations, Assumption 2(b1), we have*

$$\mathbb{P} \left(\left\| \frac{1}{T} \sum_{t=2}^T \mathbf{y}_{t-1} \epsilon_{it} \right\|_{\max} > x \right) \leq C_5 \frac{N}{x^d T^{d/2}}.$$

(b) *Under exponential tail decay of the innovations, Assumption 2(b2), we have*

$$\mathbb{P} \left(\left\| \frac{1}{T} \sum_{t=2}^T \mathbf{y}_{t-1} \epsilon_{it} \right\|_{\max} > x \right) \leq C_6 N \left(1 + \frac{1}{x} \right) \exp \left(-C_7 (xT)^{1/3} \right).$$

The constants C_5 , C_6 , and C_7 are positive and independent of N and T . The exact expression can be found in the proof below.

Proof. (a) The required upper bound follows from

$$\begin{aligned} \mathbb{P} \left(\left\| \frac{1}{T} \sum_{t=2}^T \mathbf{y}_{t-1} \epsilon_{it} \right\|_{\max} > x \right) &= \mathbb{P} \left(\max_{1 \leq k \leq N} \left| \frac{1}{T} \sum_{t=2}^T y_{k,t-1} \epsilon_{it} \right| \geq x \right) \leq \sum_{k=1}^N \mathbb{P} \left(\left| \frac{1}{T} \sum_{t=2}^T y_{k,t-1} \epsilon_{it} \right| \geq x \right) \\ &\stackrel{(i)}{\leq} \frac{1}{x^d T^d} \sum_{k=1}^N \mathbb{E} \left| \sum_{t=2}^T y_{k,t-1} \epsilon_{it} \right|^d \stackrel{(ii)}{\leq} \frac{(d-1)^d}{x^d T^d} \sum_{k=1}^N \mathbb{E} \left(\sum_{t=2}^T y_{k,t-1}^2 \epsilon_{it}^2 \right)^{d/2} \stackrel{(iii)}{\leq} \frac{(d-1)^d}{x^d T^{d/2+1}} \sum_{k=1}^N \sum_{t=2}^T \|\mathbf{y}_{k,t-1} \epsilon_{it}\|_d^d \\ &\stackrel{(iv)}{\leq} \frac{(d-1)^d}{x^d} \frac{N}{T^{d/2}} (\mu_{2d} C_D C_1)^d \mu_{2d}^d, \end{aligned}$$

by (i) the Markov inequality, (ii) Burkholder-Davis-Gundy inequality, (iii) the C_r -inequality, and (iv) a combination of the Cauchy-Schwartz inequality and the moment inequalities in Assumption 2(b1). Set $C_5 = (d-1)^d (\mu_{2d} C_D C_1)^d \mu_{2d}^d$. (b) For some $C > 0$ to be decided later, we have

$$\begin{aligned} \mathbb{P} \left(\left\| \frac{1}{T} \sum_{t=2}^T \mathbf{y}_{t-1} \epsilon_{it} \right\|_{\max} > x \right) &\leq \sum_{k=1}^N \mathbb{P} \left(\left| \sum_{t=2}^T y_{k,t-1} \epsilon_{it} \right| \geq xT \right) \\ &\leq \sum_{k=1}^N \mathbb{P} \left(\left| \sum_{t=2}^T y_{k,t-1} \epsilon_{it} \mathbb{1}_{\{|y_{k,t-1} \epsilon_{it}| \leq C\}} \right| \geq \frac{xT}{2} \right) + \sum_{k=1}^N \frac{2}{xT} \mathbb{E} \left(\left| \sum_{t=2}^T y_{k,t-1} \epsilon_{it} \mathbb{1}_{\{|y_{k,t-1} \epsilon_{it}| > C\}} \right| \right) \\ &\leq 2N \exp \left(-\frac{x^2 T}{8C^2} \right) + \frac{2}{xT} \sum_{k=1}^N \sum_{t=2}^T \mathbb{E} \left| y_{k,t-1} \epsilon_{it} \mathbb{1}_{\{|y_{k,t-1} \epsilon_{it}| > C\}} \right|, \end{aligned} \quad (10)$$

where the first term was bounded using the Azuma-Hoeffding inequality. Subsequently, using Cauchy-Schwartz on the expectation in the RHS,

$$\begin{aligned} \mathbb{E} \left| y_{k,t-1} \epsilon_{it} \mathbb{1}_{\{|y_{k,t-1} \epsilon_{it}| > C\}} \right| &\leq \|y_{k,t-1} \epsilon_{it}\|_2 \left[\mathbb{P}(|y_{k,t-1} \epsilon_{it}| > C) \right]^{1/2} \\ &\leq \|y_{k,t-1}\|_4 \|\epsilon_{it}\|_4 \left[\mathbb{P}(|y_{k,t-1}| > \sqrt{C}) + \mathbb{P}(|\epsilon_{it}| > \sqrt{C}) \right]^{1/2}. \end{aligned}$$

With exponential tail decay, we can bound moments and tail probabilities (see, e.g. page 95 in van der Vaart and Wellner (1996) and Exercise 2.18 in Wainwright (2019), and combine with Lemma S1). The resulting bound is

$$\begin{aligned} \mathbb{E} \left| y_{k,t-1} \epsilon_{it} \mathbb{1}_{\{|y_{k,t-1} \epsilon_{it}| > C\}} \right| &\leq (4!)^2 \mu_\infty^2 c_{DC1} [2 \exp(-C/\mu_\infty c_{DC1}) + 2 \exp(-C/\mu_\infty)]^{1/2} \\ &\leq 2(4!)^2 \mu_\infty^2 c_{DC1} \exp(-C/2\mu_\infty(1+c_{DC1})), \end{aligned}$$

and (10) can be continued as

$$\mathbb{P} \left(\left\| \frac{1}{T} \sum_{t=2}^T \mathbf{y}_{t-1} \epsilon_{it} \right\|_{max} > x \right) \leq 2N \exp\left(-\frac{x^2 T}{8C^2}\right) + 4(4!)^2 \mu_\infty^2 c_{DC1} \frac{N}{x} \exp\left(-\frac{C}{2\mu_\infty(1+c_{DC1})}\right).$$

The choice $C = (\frac{1}{4}\mu_\infty(1+c_{DC}+1)xT)^{1/3}$ sets the exponents equal, and for this C we find

$$\mathbb{P} \left(\left\| \frac{1}{T} \sum_{t=2}^T \mathbf{y}_{t-1} \epsilon_{it} \right\|_{max} > x \right) \leq (2 + 4(4!)^2 \mu_\infty^2 c_{DC1}) N \left(1 + \frac{1}{x}\right) \exp\left(-\left(\frac{xT}{128[\mu_\infty(1+c_{DC1})]^2}\right)^{\frac{1}{3}}\right).$$

This establishes the desired result with $C_6 = (2 + 4(4!)^2 \mu_\infty^2 c_{DC1})$ and $C_7 = (128[\mu_\infty(1+c_{DC1})]^2)^{-1/3}$. \square

Appendix B Proofs of Main Results

Proof of Theorem 1. We first prove various intermediate results, see (a)–(d) below. We afterwards combine these results and recover Theorem 1.

(a) The matrix $\tilde{\mathbf{C}}_s = \left(\sum_{j=0}^{s-1} \mathbf{A}^j\right) \mathbf{B} =: \tilde{\mathbf{D}}_s \mathbf{B}$ has a maximum bandwidth of $(s+1)(k_0-1)+1$ and satisfies

$$\left\| \tilde{\mathbf{C}}_s - \mathbf{C} \right\|_{\text{F}} \leq C_1 \delta_A^s.$$

(b) Define $\boldsymbol{\Sigma}_0^{r,s} = \sum_{j=0}^r \tilde{\mathbf{C}}_s^j \tilde{\mathbf{D}}_s \boldsymbol{\Sigma}_\epsilon \tilde{\mathbf{D}}_s' (\tilde{\mathbf{C}}_s')^j$ with $\tilde{\mathbf{C}}_s$ as in Theorem 1(a). The matrix $\boldsymbol{\Sigma}_0^{r,s}$ is a banded matrix with bandwidth no larger than $2(rs+r+s)(k_0-1)+2l_0+1$. Moreover,

$$\left\| \boldsymbol{\Sigma}_0^{r,s} - \boldsymbol{\Sigma}_0 \right\|_{\text{F}} \leq C_2 \left(\frac{\delta_A^s}{[1 - (C_1 \delta_A^s + \delta_C)^2]^3} + \delta_C^{2(r+1)} \right),$$

whenever s is large enough such that $C_1 \delta_A^s + \delta_C < 1$.

(c) Define $\boldsymbol{\Sigma}_1^{r,s} = \tilde{\mathbf{C}}_s \boldsymbol{\Sigma}_0^{r,s}$ with $\tilde{\mathbf{C}}_s$ and $\boldsymbol{\Sigma}_0^{r,s}$ as in Theorems 1(a) and 1(b), respectively. The matrix $\boldsymbol{\Sigma}_1^{r,s}$ is a banded matrix with bandwidth no larger than $(2rs+2r+3s+1)(k_0-1)+2l_0+1$. Moreover,

$$\left\| \boldsymbol{\Sigma}_1^{r,s} - \boldsymbol{\Sigma}_1 \right\|_{\text{F}} \leq C_3 \left(\frac{\delta_A^s}{[1 - (C_1 \delta_A^s + \delta_C)^2]^3} + \delta_C^{2(r+1)} \right),$$

whenever s is large enough such that $C_1 \delta_A^s + \delta_C < 1$.

(d) Take any $h_1 \geq 2(rs + r + s)(k_0 - 1) + 2l_0 + 1$, then

$$\|\mathcal{B}_{h_1}(\widehat{\boldsymbol{\Sigma}}_0) - \boldsymbol{\Sigma}_0\|_2 \leq \epsilon + 2C_2(h_1 + 1) \left(\frac{\delta_A^s}{[1 - (C_1\delta_A^s + \delta_C)^2]^3} + \delta_C^{2(r+1)} \right),$$

with a probability of at least $1 - \mathcal{P}_1(\epsilon, N, T)$ (for polynomial tail decay) or $1 - \mathcal{P}_2(\epsilon, N, T)$ (for exponential tail decay).

(e) Take any $h_2 \geq (2rs + 2r + 3s + 1)(k_0 - 1) + 2l_0 + 1$, then

$$\|\mathcal{B}_{h_2}(\widehat{\boldsymbol{\Sigma}}_1) - \boldsymbol{\Sigma}_1\|_2 \leq \epsilon + 2C_3(h_2 + 1) \left(\frac{\delta_A^s}{[1 - (C_1\delta_A^s + \delta_C)^2]^3} + \delta_C^{2(r+1)} \right),$$

with a probability of at least $1 - \mathcal{P}_1(\epsilon, N, T)$ (for polynomial tail decay) or $1 - \mathcal{P}_2(\epsilon, N, T)$ (for exponential tail decay).

Explicit expressions for C_1, C_2, C_3 , and $0 \leq \delta_C < 1$ are provided in the proofs below.

(a) The proof builds upon results from Guo et al. (2016) on banded vector autoregressions. Recall that $\mathbf{C} = \mathbf{D}\mathbf{B}$ with $\mathbf{D} = (\mathbf{I}_N - \mathbf{A})^{-1}$. $\widetilde{\mathbf{D}}_s = \sum_{j=0}^{s-1} \mathbf{A}^j$ has a bandwidth of at most $s(k_0 - 1) + 1$ and satisfies¹¹

$$\|\widetilde{\mathbf{D}}_s - \mathbf{D}\|_{\text{F}} = \left\| \sum_{j=0}^{s-1} \mathbf{A}^j - (\mathbf{I}_N - \mathbf{A})^{-1} \right\|_{\text{F}} = \left\| -\sum_{j=s}^{\infty} \mathbf{A}^j \right\|_{\text{F}} \leq \sum_{j=s}^{\infty} \|\mathbf{A}\|_{\text{F}}^j \leq \frac{\delta_A^s}{1 - \delta_A}.$$

The product $\widetilde{\mathbf{C}}_s = \widetilde{\mathbf{D}}_s \mathbf{B}$ has a maximal bandwidth of $(s + 1)(k_0 - 1) + 1$. Since $\|\mathbf{B}\|_{\text{F}} \leq C_B$ (Assumption 3(c)), we also have

$$\|\widetilde{\mathbf{C}}_s - \mathbf{C}\|_{\text{F}} = \left\| (\widetilde{\mathbf{D}}_s - \mathbf{D}) \mathbf{B} \right\|_{\text{F}} \leq \|\widetilde{\mathbf{D}}_s - \mathbf{D}\|_{\text{F}} \|\mathbf{B}\|_{\text{F}} \leq C_B \frac{\delta_A^s}{1 - \delta_A}.$$

and the claim follows with $C_1 = \frac{C_B}{1 - \delta_A}$. (b) Iterating on the observation in footnote 11, we conclude that the bandwidth of $\widetilde{\mathbf{C}}_s^r$ is at most $r[(s + 1)(k_0 - 1) + 1] - (r - 1) = r(s + 1)(k_0 - 1) + 1$. The bandwidth of $\boldsymbol{\Sigma}_0^{r,s}$ therefore does not exceed

$$2[r(s + 1)(k_0 - 1) + 1] + 2(s(k_0 - 1) + 1) + (2l_0 + 1) - 4 = 2(rs + r + s)(k_0 - 1) + 2l_0 + 1.$$

We now bound $\|\boldsymbol{\Sigma}_0^{r,s} - \boldsymbol{\Sigma}_0\|_{\text{F}}$. Assumption 1(b), imposes $\|\mathbf{C}\|_{\text{F}} \leq \delta_C$ for some $0 \leq \delta_C < 1$. Because $\boldsymbol{\Sigma}_0 = \sum_{j=0}^{\infty} \mathbf{C}^j \mathbf{D} \boldsymbol{\Sigma}_\epsilon \mathbf{D}' (\mathbf{C}')^j$, it holds that

$$\begin{aligned} \|\boldsymbol{\Sigma}_0^{r,s} - \boldsymbol{\Sigma}_0\|_{\text{F}} &= \left\| \sum_{j=0}^r [\widetilde{\mathbf{C}}_s^j \widetilde{\mathbf{D}}_s \boldsymbol{\Sigma}_\epsilon \widetilde{\mathbf{D}}_s' (\widetilde{\mathbf{C}}_s')^j - \mathbf{C}^j \mathbf{D} \boldsymbol{\Sigma}_\epsilon \mathbf{D}' (\mathbf{C}')^j] - \sum_{j=r+1}^{\infty} \mathbf{C}^j \mathbf{D} \boldsymbol{\Sigma}_\epsilon \mathbf{D}' (\mathbf{C}')^j \right\|_{\text{F}} \\ &\leq \sum_{j=0}^r \|\boldsymbol{\Sigma}_\epsilon\|_{\text{F}} \|\widetilde{\mathbf{C}}_s^j\|_{\text{F}}^2 \|\widetilde{\mathbf{D}}_s - \mathbf{D}\|_{\text{F}}^2 + 2 \sum_{j=0}^r \|\boldsymbol{\Sigma}_\epsilon\|_{\text{F}} \|\widetilde{\mathbf{C}}_s^j\|_{\text{F}}^2 \|\mathbf{D}\|_{\text{F}} \|\widetilde{\mathbf{D}}_s - \mathbf{D}\|_{\text{F}}^2 \\ &\quad + \sum_{j=1}^r \|\boldsymbol{\Sigma}_\epsilon\|_{\text{F}} \|\widetilde{\mathbf{C}}_s^j - \mathbf{C}^j\|_{\text{F}}^2 \|\mathbf{D}\|_{\text{F}}^2 + 2 \sum_{j=1}^r \|\boldsymbol{\Sigma}_\epsilon\|_{\text{F}} \|\widetilde{\mathbf{C}}_s^j - \mathbf{C}^j\|_{\text{F}} \|\mathbf{C}^j\|_{\text{F}} \|\mathbf{D}\|_{\text{F}}^2 \\ &\quad + \left\| \sum_{j=r+1}^{\infty} \mathbf{C}^j \mathbf{D} \boldsymbol{\Sigma}_\epsilon \mathbf{D}' (\mathbf{C}')^j \right\|_{\text{F}}. \end{aligned} \tag{11}$$

¹¹If matrices \mathbf{F}_1 and \mathbf{F}_2 are banded matrices with bandwidths k_1 and k_2 , respectively, then the product $\mathbf{F}_1 \mathbf{F}_2$ is again a banded matrix with a bandwidth of at most $k_1 + k_2 - 1$.

An inspection of (11) shows that additional upper bounds are required on $\|\tilde{\mathbf{C}}_s^j\|_{\Gamma}$, $\|\mathbf{C}^j - \tilde{\mathbf{C}}_s^j\|_{\Gamma}$, and $\|\sum_{j=r+1}^{\infty} \mathbf{C}^j \mathbf{D} \Sigma_{\epsilon} \mathbf{D}' (\mathbf{C}')^j\|_{\Gamma}$. For $\|\tilde{\mathbf{C}}_s^j\|_{\Gamma}$, using properties of matrix norms and Theorem 1(a), we obtain

$$\|\tilde{\mathbf{C}}_s^j\|_{\Gamma} = \left\| (\tilde{\mathbf{C}}_s - \mathbf{C} + \mathbf{C})^j \right\|_{\Gamma} \leq \left(\|\tilde{\mathbf{C}}_s - \mathbf{C}\|_{\Gamma} + \|\mathbf{C}\|_{\Gamma} \right)^j \leq [C_1 \delta_A^s + \delta_C]^j. \quad (12)$$

Furthermore, expanding the matrix powers provides

$$\begin{aligned} \|\mathbf{C}^j - \tilde{\mathbf{C}}_s^j\|_{\Gamma} &= \left\| \mathbf{C}^j - (\tilde{\mathbf{C}}_s - \mathbf{C} + \mathbf{C})^j \right\|_{\Gamma} \\ &= \left\| \mathbf{C}^j - \left((\tilde{\mathbf{C}}_s - \mathbf{C})^j + (\tilde{\mathbf{C}}_s - \mathbf{C})^{j-1} \mathbf{C} + (\tilde{\mathbf{C}}_s - \mathbf{C})^{j-2} \mathbf{C} (\tilde{\mathbf{C}}_s - \mathbf{C}) + \dots + \mathbf{C} (\tilde{\mathbf{C}}_s - \mathbf{C})^{j-1} \dots + \mathbf{C}^j \right) \right\|_{\Gamma} \\ &\leq \sum_{k=1}^j \binom{j}{k} \|\mathbf{C}\|_{\Gamma}^{j-k} \|\tilde{\mathbf{C}}_s - \mathbf{C}\|_{\Gamma}^k = \sum_{k=0}^{j-1} \binom{j}{k+1} \|\mathbf{C}\|_{\Gamma}^{(j-1)-k} \|\tilde{\mathbf{C}}_s - \mathbf{C}\|_{\Gamma}^{k+1} \\ &= \|\tilde{\mathbf{C}}_s - \mathbf{C}\|_{\Gamma} \sum_{k=0}^{j-1} \frac{j}{k+1} \binom{j-1}{k} \|\mathbf{C}\|_{\Gamma}^{(j-1)-k} \|\tilde{\mathbf{C}}_s - \mathbf{C}\|_{\Gamma}^k \leq C_1 j \delta_A^s \left[\|\tilde{\mathbf{C}}_s - \mathbf{C}\|_{\Gamma} + \|\mathbf{C}\|_{\Gamma} \right]^{j-1} \\ &\leq C_1 j \delta_A^s [C_1 \delta_A^s + \delta_C]^{j-1} \end{aligned} \quad (13)$$

Finally, since $\|\Sigma_{\epsilon}\|_{\Gamma} \leq C_{\epsilon}$ and $\|\mathbf{D}\|_{\Gamma} = \left\| \sum_{j=0}^{\infty} \mathbf{A}^j \right\|_{\Gamma} = \sum_{j=0}^{\infty} \|\mathbf{A}\|_{\Gamma}^j \leq c_D$ (Assumption 1(a)), we have

$$\left\| \sum_{j=r+1}^{\infty} \mathbf{C}^j \mathbf{D} \Sigma_{\epsilon} \mathbf{D}' (\mathbf{C}')^j \right\|_{\Gamma} \leq \sum_{j=r+1}^{\infty} \|\Sigma_{\epsilon}\|_{\Gamma} \|\mathbf{D}\|_{\Gamma}^2 \|\mathbf{C}\|_{\Gamma}^{2j} \leq C_{\epsilon} c_D^2 \sum_{j=r+1}^{\infty} \delta_C^{2j} = C_{\epsilon} c_D^2 \frac{\delta_C^{2(r+1)}}{1 - \delta_C^2}. \quad (14)$$

Returning to (11) and inserting the upper bounds in (12)–(14), we find

$$\begin{aligned} \|\Sigma_0^{r,s} - \Sigma_0\|_{\Gamma} &\leq \frac{C_{\epsilon}}{(1 - \delta_A)^2} \delta_A^{2s} \sum_{j=0}^r (C_1 \delta_A^s + \delta_C)^{2j} + 2 \frac{C_{\epsilon} c_D}{(1 - \delta_A)^2} \delta_A^{2s} \sum_{j=0}^r (C_1 \delta_A^s + \delta_C)^{2j} \\ &\quad + C_{\epsilon} C_1^2 c_D^2 \delta_A^{2s} \sum_{j=1}^r j^2 (C_1 \delta_A^s + \delta_C)^{2(j-1)} + 2 C_{\epsilon} C_1 c_D^2 \delta_A^s \sum_{j=1}^r j \delta_C^j (C_1 \delta_A^s + \delta_C)^{j-1} + C_{\epsilon} c_D^2 \frac{\delta_C^{2(r+1)}}{1 - \delta_C^2}. \end{aligned}$$

Assuming s is sufficient large, that is assuming $C_1 \delta_A^s + \delta_C < 1$, we subsequently use result on geometric series and conclude¹²

$$\begin{aligned} \|\Sigma_0^{r,s} - \Sigma_0\|_{\Gamma} &\leq \frac{C_{\epsilon}}{(1 - \delta_A)^2} \delta_A^{2s} \frac{1}{1 - (C_1 \delta_A^s + \delta_C)^2} + 2 \frac{C_{\epsilon} c_D}{(1 - \delta_A)^2} \delta_A^{2s} \frac{1}{1 - (C_1 \delta_A^s + \delta_C)^2} \\ &\quad + \frac{C_{\epsilon} C_1^2 c_D^2 \delta_A^{2s}}{(C_1 \delta_A^s + \delta_C)^2} \frac{(C_1 \delta_A^s + \delta_C)^2}{[1 - (C_1 \delta_A^s + \delta_C)^2]^3} + 2 \frac{C_{\epsilon} C_1 c_D^2 \delta_A^s}{C_1 \delta_A^s + \delta_C} \frac{\delta_C (C_1 \delta_A^s + \delta_C)}{[1 - \delta_C (C_1 \delta_A^s + \delta_C)]^2} + C_{\epsilon} c_D^2 \frac{\delta_C^{2(r+1)}}{1 - \delta_C^2} \\ &= \frac{C_{\epsilon}}{(1 - \delta_A)^2} \frac{1}{1 - (C_1 \delta_A^s + \delta_C)^2} \delta_A^{2s} + 2 \frac{C_{\epsilon} c_D}{(1 - \delta_A)^2} \frac{1}{1 - (C_1 \delta_A^s + \delta_C)^2} \delta_A^{2s} + \frac{C_{\epsilon} C_1^2 c_D^2}{[1 - (C_1 \delta_A^s + \delta_C)^2]^3} \delta_A^{2s} \\ &\quad + 2 \frac{C_{\epsilon} C_1 c_D^2 \delta_C}{[1 - \delta_C (C_1 \delta_A^s + \delta_C)]^2} \delta_A^s + C_{\epsilon} c_D^2 \frac{\delta_C^{2(r+1)}}{1 - \delta_C^2} \\ &\leq \frac{1}{(1 - \delta_A)^2} \frac{C_{\epsilon} + 2 C_{\epsilon} c_D}{1 - (C_1 \delta_A^s + \delta_C)^2} \delta_A^{2s} + \frac{C_{\epsilon} C_1^2 c_D^2 + 2 C_{\epsilon} C_1 c_D^2 \delta_C}{[1 - (C_1 \delta_A^s + \delta_C)^2]^3} \delta_A^s + \frac{C_{\epsilon} c_D^2}{1 - \delta_C^2} \delta_C^{2(r+1)} \\ &\leq \left[\frac{C_{\epsilon} + 2 C_{\epsilon} c_D}{(1 - \delta_A)^2} + C_{\epsilon} C_1^2 c_D^2 + 2 C_{\epsilon} C_1 c_D^2 \delta_C \right] \frac{\delta_A^s}{[1 - (C_1 \delta_A^s + \delta_C)^2]^3} + \frac{C_{\epsilon} c_D^2}{1 - \delta_C^2} \delta_C^{2(r+1)}. \end{aligned}$$

¹²Specifically, $\sum_{j=1}^{\infty} j z^j = \frac{z}{(1-z)^2}$ and $\sum_{j=1}^{\infty} j^2 z^j = \frac{z}{(1-z)^3}$ for $|z| < 1$.

The claim is thus indeed valid with $C_2 = \max \left\{ \frac{C_\epsilon + 2C_\epsilon c_D}{(1-\delta_A)^2} + C_\epsilon C_1^2 c_D^2 + 2C_\epsilon C_1 c_D^2 \delta_C, \frac{C_\epsilon c_D^2}{1-\delta_C^2} \right\}$. **(c)** We have $\Sigma_1 = (I_N - A)^{-1} B \Sigma_0 = C \Sigma_0$, and hence

$$\|\Sigma_1^{r,s} - \Sigma_1\|_{\perp} = \left\| \tilde{C}_s(\Sigma_0^{r,s} - \Sigma_0) + (\tilde{C}_s - C)\Sigma_0 \right\|_{\perp} \leq \left\| \tilde{C}_s \right\|_{\perp} \|\Sigma_0^{r,s} - \Sigma_0\|_{\perp} + \left\| \tilde{C}_s - C \right\|_{\perp} \|\Sigma_0\|_{\perp} \quad (15)$$

Now combine $\left\| \tilde{C}_s \right\|_{\perp} \leq C_1 \delta_\kappa^s + \delta_C \leq 1$ (since s is taken sufficiently large), Theorem 1(b), (13) with $j = 1$, and $\|\Sigma_0\|_{\perp} \leq \sum_{j=0}^{\infty} \|C^j D \Sigma_\epsilon D' (C')^j\|_{\perp} \leq \frac{C_\epsilon c_D^2}{1-\delta_C^2}$ to obtain the stated result with $C_3 = C_2 + \frac{C_1 C_\epsilon c_D^2}{1-\delta_C^2}$. **(d)** We have

$$\begin{aligned} \left\| \mathcal{B}_{h_1}(\hat{\Sigma}_0) - \Sigma_0 \right\|_{\perp} &\leq \left\| \mathcal{B}_{h_1}(\hat{\Sigma}_0) - \mathcal{B}_{h_1}(\Sigma_0) \right\|_{\perp} + \left\| \mathcal{B}_{h_1}(\Sigma_0) - \mathcal{B}_{h_1}(\Sigma_0^{r,s}) \right\|_{\perp} + \left\| \mathcal{B}_{h_1}(\Sigma_0^{r,s}) - \Sigma_0 \right\|_{\perp} \\ &= \left\| \mathcal{B}_{h_1}(\hat{\Sigma}_0 - \Sigma_0) \right\|_{\perp} + \left\| \mathcal{B}_{h_1}(\Sigma_0 - \Sigma_0^{r,s}) \right\|_{\perp} + \left\| \Sigma_0^{r,s} - \Sigma_0 \right\|_{\perp}, \end{aligned} \quad (16)$$

because $\Sigma_0^{r,s}$ is a banded matrix already. We consider the three terms in the RHS of (16) separately. First, there are at most $2h_1 + 1$ nonzero elements in any column/row of $\mathcal{B}_{h_1}(\hat{\Sigma}_0 - \Sigma_0)$ and thus

$$\left\| \mathcal{B}_{h_1}(\hat{\Sigma}_0 - \Sigma_0) \right\|_{\perp} \leq (2h_1 + 1) \left\| \hat{\Sigma}_0 - \Sigma_0 \right\|_{max} \quad (17)$$

and

$$\begin{aligned} \mathbb{P} \left(\left\| \mathcal{B}_{h_1}(\hat{\Sigma}_0 - \Sigma_0) \right\|_{\perp} \leq x \right) &\geq \mathbb{P} \left((2h_1 + 1) \left\| \hat{\Sigma}_0 - \Sigma_0 \right\|_{max} \leq x \right) = 1 - \mathbb{P} \left(\left\| \hat{\Sigma}_0 - \Sigma_0 \right\|_{max} > \frac{x}{2h_1 + 1} \right) \\ &\geq 1 - \mathbb{P} \left(\bigcup_{1 \leq i, j \leq N} \left[\hat{\Sigma}_0 - \Sigma_0 \right]_{ij} > \frac{x}{2h_1 + 1} \right) \geq 1 - \sum_{i=1}^N \sum_{j=1}^N \mathbb{P} \left(\left| \sum_{t=2}^T x_{it} x_{jt} - \mathbb{E}(x_{it} x_{jt}) \right| > \frac{Tx}{2h_1 + 1} \right) \\ &\geq \begin{cases} 1 - N^2 \left[\left(b_1 T^{(1-\delta)/3} + \frac{(2h_1+1)b_3}{x} \right) \exp \left(-\frac{T^{(1-\delta)/3}}{2b_1^2} \right) + \frac{b_2(2h_1+1)^d}{x^d T^{\frac{\delta}{2}(d-1)}} \right] & \text{(polynomial tails),} \\ 1 - N^2 \left[\frac{\beta_1(2h_1+1)}{x} + \frac{2}{\beta_2} \left(\frac{Tx^2}{(2h_1+1)^2} \right)^{1/7} \right] \exp \left(-\frac{1}{\beta_3} \left(\frac{Tx^2}{(2h_1+1)^2} \right)^{1/7} \right) & \text{(exponential tails),} \end{cases} \end{aligned} \quad (18)$$

where the last inequality exploits Lemma S3 (see Supplement). Note that the probabilities in (18) coincide with the probabilities defined as $1 - \mathcal{P}_1(x, N, T)$ and $1 - \mathcal{P}_2(x, N, T)$ in Theorem 1. Second, using $\|\cdot\|_{max} \leq \|\cdot\|_{\perp}$, we have $\left\| \mathcal{B}_{h_1}(\Sigma_0 - \Sigma_0^{r,s}) \right\|_{\perp} \leq (2h_1 + 1) \left\| \Sigma_0 - \Sigma_0^{r,s} \right\|_{max} \leq (2h_1 + 1) \left\| \Sigma_0^{r,s} - \Sigma_0 \right\|_{\perp}$. Overall, if $\left\| \mathcal{B}_{h_1}(\hat{\Sigma}_0 - \Sigma_0) \right\|_{\perp} \leq \epsilon$ holds, then continuing from (16),

$$\left\| \mathcal{B}_{h_1}(\hat{\Sigma}_0) - \Sigma_0 \right\|_{\perp} \leq \epsilon + 2(h_1 + 1) \left\| \Sigma_0^{r,s} - \Sigma_0 \right\|_{\perp} \leq \epsilon + 2C_2 N \left(\frac{\delta_A^s}{[1 - (C_1 \delta_A^s + \delta_C)^2]^3} + \delta_C^{2(r+1)} \right),$$

where the last inequality follows from part (b) of this proof and the fact that $h_1 + 1 \leq N$. A lower bound on the probability of $\left\{ \left\| \mathcal{B}_{h_1}(\hat{\Sigma}_0 - \Sigma_0) \right\|_{\perp} \leq \epsilon \right\}$ occurring is immediately available from (18). **(e)** Mimicking the steps from (d), we find

$$\left\| \mathcal{B}_{h_2}(\hat{\Sigma}_1) - \Sigma_1 \right\|_{\perp} \leq \epsilon + 2(h_2 + 1) \left\| \Sigma_1^{r,s} - \Sigma_1 \right\|_{\perp} \leq \epsilon + 2C_3 N \left(\frac{\delta_A^s}{[1 - (C_1 \delta_A^s + \delta_C)^2]^3} + \delta_C^{2(r+1)} \right)$$

if we use part (c) and if $\left\{ \left\| \mathcal{B}_{h_2}(\hat{\Sigma}_1 - \Sigma_1) \right\|_{\perp} \leq \epsilon \right\}$ holds. The probability of the latter event is $1 - \mathcal{P}_1(\epsilon, N, T)$ (polynomial tails) or $1 - \mathcal{P}_2(\epsilon, N, T)$ (exponential tails).

We now combine all these intermediate results to recover the result from the theorem. Parts (d) and (e) are both applicable since $h = \max\{h_1, h_2\}$. Lemma S4 implies that

$$\begin{aligned} \left\| \widehat{\mathbf{V}}_h - \mathbf{V} \right\|_{\cdot} &\leq \left\| \mathcal{B}_{h_2}(\widehat{\boldsymbol{\Sigma}}_1) - \boldsymbol{\Sigma}_1 \right\|_{\cdot} + \left\| \mathcal{B}_{h_1}(\widehat{\boldsymbol{\Sigma}}_0) - \boldsymbol{\Sigma}_0 \right\|_{\cdot} \\ &\leq 2\epsilon + 2C_4N \left(\frac{\delta_{\kappa}^s}{[1 - (C_1\delta_{\kappa}^s + \delta_C)^2]^3} + \delta_C^{2(r+1)} \right), \end{aligned}$$

when $\left\{ \left\| \mathcal{B}_{h_2}(\widehat{\boldsymbol{\Sigma}}_1) - \boldsymbol{\Sigma}_1 \right\|_{\cdot} \leq \epsilon \right\} \cap \left\{ \left\| \mathcal{B}_{h_1}(\widehat{\boldsymbol{\Sigma}}_0) - \boldsymbol{\Sigma}_0 \right\|_{\cdot} \leq \epsilon \right\}$ takes place and $C_4 = C_2 + C_3$. From $\mathbb{P}(A \cap B) = 1 - \mathbb{P}(A^c \cup B^c) \geq 1 - \mathbb{P}(A^c) - \mathbb{P}(B^c)$ it follows that this joint event takes place with probabilities $1 - 2\mathcal{P}_1(\epsilon, N, T)$ and $1 - 2\mathcal{P}_2(\epsilon, N, T)$ in the cases of polynomial and exponential tail decay, respectively.

It remains to determine s and r such that $C_4N\delta_A^s/[1 - (C_1\delta_A^s + \delta_C)^2]^3 \leq \epsilon$ and $C_4N\delta_C^{2(r+1)} \leq \epsilon$ hold. For any $s \geq s^*$ with $s^* = \log\left(\frac{1}{C_1}[(1 - (1 - \delta_C)^{1/3})^{1/2} - \delta_C]\right)/\log(\delta_A)$, we have $1/[1 - (C_1\delta_A^s + \delta_C)^2]^3 \leq 1/[1 - \delta_C]$. Under the latter assumption, we determine the s such that

$$\frac{C_4N\delta_A^s}{1 - \delta_C} \leq \epsilon \iff s \log(\delta_A) \leq \log\left(\frac{(1 - \delta_C)\epsilon}{C_4N}\right) \iff s \geq \frac{\log(C_4N/(1 - \delta_C)\epsilon)}{|\log(\delta_A)|}.$$

Similarly, for r , the choice $r = \log(C_4N/\epsilon)/2|\log(\delta_C)|$ suffices. \square

Proof of Theorem 2. The proof of the theorem relies on the properties of dual norms. Recall $P_{\alpha}(\mathbf{c}) = \alpha \sum_{g \in \mathcal{G}} \sqrt{|g|} \|\mathbf{c}_g\|_2 + (1 - \alpha) \|\mathbf{c}\|_1$. Exploiting the properties of $\|\cdot\|_1$ and $\|\cdot\|_2$, it is straightforward to verify that $P_{\alpha}(\cdot)$ is a norm for any $0 \leq \alpha \leq 1$. For any norm $\|\cdot\|$, we define its dual norm $\|\cdot\|^*$ through $\|\mathbf{c}\|^* = \sup_{\mathbf{x} \neq \mathbf{0}} \frac{|\mathbf{c}'\mathbf{x}|}{\|\mathbf{x}\|}$. The dual-norm inequality states that

$$\mathbf{c}'\mathbf{x} \leq \|\mathbf{c}\|^* \|\mathbf{x}\| \quad \text{for all conformable vectors } \mathbf{c} \text{ and } \mathbf{x}. \quad (19)$$

For the norm $P_{\alpha}(\mathbf{c})$, its dual norm $P_{\alpha}^*(\mathbf{c})$ is bounded by

$$\begin{aligned} P_{\alpha}^*(\mathbf{c}) &= \sup_{\mathbf{x} \neq \mathbf{0}} \frac{|\mathbf{c}'\mathbf{x}|}{P_{\alpha}(\mathbf{x})} = \sup_{\mathbf{x} \neq \mathbf{0}} \frac{|\mathbf{c}'\mathbf{x}|}{\alpha \sum_{g \in \mathcal{G}} \sqrt{|g|} \|\mathbf{x}_g\|_2 + (1 - \alpha) \|\mathbf{x}\|_1} \\ &\stackrel{(i)}{\leq} \alpha \sup_{\mathbf{x} \neq \mathbf{0}} \frac{|\mathbf{c}'\mathbf{x}|}{\sum_{g \in \mathcal{G}} \sqrt{|g|} \|\mathbf{x}_g\|_2} + (1 - \alpha) \sup_{\mathbf{x} \neq \mathbf{0}} \frac{|\mathbf{c}'\mathbf{x}|}{\|\mathbf{x}\|_1} \stackrel{(ii)}{\leq} \alpha \max_{g \in \mathcal{G}} \frac{\|\mathbf{c}_g\|_2}{\sqrt{|g|}} + (1 - \alpha) \|\mathbf{c}\|_{\infty}, \end{aligned} \quad (20)$$

by convexity of the function $f(x) = x^{-1}$ in step (i), and using for step (ii) both $\|\mathbf{c}\|_1^* = \|\mathbf{c}\|_{\infty}$ and

$$\begin{aligned} \sup_{\mathbf{x} \neq \mathbf{0}} \frac{|\mathbf{c}'\mathbf{x}|}{\sum_{g \in \mathcal{G}} \sqrt{|g|} \|\mathbf{x}_g\|_2} &= \sup_{\mathbf{x} \neq \mathbf{0}, \sum_{g \in \mathcal{G}} \sqrt{|g|} \|\mathbf{x}_g\|_2 = 1} \left| \sum_{g \in \mathcal{G}} \mathbf{c}'_g \mathbf{x}_g \right| \\ &\leq \sup_{\mathbf{x} \neq \mathbf{0}, \sum_{g \in \mathcal{G}} \sqrt{|g|} \|\mathbf{x}_g\|_2 = 1} \sum_{g \in \mathcal{G}} \left\| \frac{\mathbf{c}_g}{\sqrt{|g|}} \right\|_2 \|\sqrt{|g|} \mathbf{x}_g\|_2 \leq \max_{g \in \mathcal{G}} \frac{\|\mathbf{c}_g\|_2}{\sqrt{|g|}}. \end{aligned}$$

We now start the actual proof. Recall $\hat{\boldsymbol{\sigma}}_h = \text{vec}\left(\mathcal{B}_h(\widehat{\boldsymbol{\Sigma}}_1)'\right)$, $\widehat{\mathbf{V}}_h = [\mathcal{B}_h(\widehat{\boldsymbol{\Sigma}}_1)' \quad \mathcal{B}_h(\widehat{\boldsymbol{\Sigma}}_0)']$, $\mathbf{V} = [\boldsymbol{\Sigma}'_1 \quad \boldsymbol{\Sigma}_0']$, and $\mathbf{C} = [\mathbf{A} \quad \mathbf{B}]$. Then,

$$\begin{aligned} \hat{\boldsymbol{\sigma}}_h - \widehat{\mathbf{V}}_h^{(d)} \mathbf{c} &= \text{vec}\left(\mathcal{B}_h(\widehat{\boldsymbol{\Sigma}}_1)' - \widehat{\mathbf{V}}_h \mathbf{C}'\right) = \text{vec}\left(\left[\mathcal{B}_h(\widehat{\boldsymbol{\Sigma}}_1) - \boldsymbol{\Sigma}_1\right]' - \left[\widehat{\mathbf{V}}_h - \mathbf{V}\right] \mathbf{C}' + \underbrace{[\boldsymbol{\Sigma}'_1 - \mathbf{V} \mathbf{C}']}_{=\mathbf{0}, \text{ see (3)}}\right) \\ &= \underbrace{\text{vec}\left(\mathcal{B}_h(\widehat{\boldsymbol{\Sigma}}_1)' - \boldsymbol{\Sigma}'_1\right)}_{\hat{\boldsymbol{\Delta}}_{\Sigma}} - \underbrace{\left[\widehat{\mathbf{V}}_h^{(d)} - \mathbf{V}^{(d)}\right]}_{\hat{\boldsymbol{\Delta}}_{\mathbf{V}}} \mathbf{c} = \hat{\boldsymbol{\Delta}}_{\Sigma} - \hat{\boldsymbol{\Delta}}_{\mathbf{V}} \mathbf{c}, \end{aligned} \quad (21)$$

Using (21), we rewrite

$$\begin{aligned} \left\| \hat{\boldsymbol{\sigma}}_h - \hat{\mathbf{V}}_h^{(d)} \hat{\mathbf{c}} \right\|_2^2 &= \left\| \left[\hat{\boldsymbol{\sigma}}_h - \hat{\mathbf{V}}_h^{(d)} \mathbf{c} \right] - \left[\hat{\mathbf{V}}_h^{(d)} (\hat{\mathbf{c}} - \mathbf{c}) \right] \right\|_2^2 \\ &= \left\| \hat{\boldsymbol{\sigma}}_h - \hat{\mathbf{V}}_h^{(d)} \mathbf{c} \right\|_2^2 + \left\| \hat{\mathbf{V}}_h^{(d)} (\hat{\mathbf{c}} - \mathbf{c}) \right\|_2^2 - 2 (\hat{\mathbf{c}} - \mathbf{c})' \hat{\mathbf{V}}_h^{(d)'} \left(\hat{\boldsymbol{\Delta}}_\Sigma - \hat{\boldsymbol{\Delta}}_V \mathbf{c} \right). \end{aligned}$$

Recalling the objective function $\mathcal{L}_\alpha(\mathbf{c}; \lambda) = \left\| \hat{\boldsymbol{\sigma}} - \hat{\mathbf{V}}_h^{(d)} \mathbf{c} \right\|_2^2 + \lambda P_\alpha(\mathbf{c})$ and noting that $\mathcal{L}_\alpha(\hat{\mathbf{c}}; \lambda) \leq \mathcal{L}_\alpha(\mathbf{c}; \lambda)$ by construction, it follows that

$$\begin{aligned} \left\| \hat{\mathbf{V}}_h^{(d)} (\hat{\mathbf{c}} - \mathbf{c}) \right\|_2^2 + \lambda P_\alpha(\hat{\mathbf{c}}) &\leq 2 (\hat{\mathbf{c}} - \mathbf{c})' \hat{\mathbf{V}}_h^{(d)'} \left(\hat{\boldsymbol{\Delta}}_\Sigma - \hat{\boldsymbol{\Delta}}_V \mathbf{c} \right) + \lambda P_\alpha(\mathbf{c}) \\ &\leq 2 P_\alpha(\hat{\mathbf{c}} - \mathbf{c}) P_\alpha^* \left(\hat{\mathbf{V}}_h^{(d)'} \left(\hat{\boldsymbol{\Delta}}_\Sigma - \hat{\boldsymbol{\Delta}}_V \mathbf{c} \right) \right) + \lambda P_\alpha(\mathbf{c}) \quad (22) \\ &\leq P_\alpha(\hat{\mathbf{c}} - \mathbf{c}) \left[2 P_\alpha^* \left(\hat{\mathbf{V}}_h^{(d)'} \hat{\boldsymbol{\Delta}}_\Sigma \right) + 2 P_\alpha^* \left(\hat{\mathbf{V}}_h^{(d)'} \hat{\boldsymbol{\Delta}}_V \mathbf{c} \right) \right] + \lambda P_\alpha(\mathbf{c}), \end{aligned}$$

where we used the dual-norm inequality (see (19)) and the triangle property of (dual) norms in the second and third inequality, respectively. Define the sets

$$\mathcal{H}_1(x) = \left\{ 2 P_\alpha^* \left(\hat{\mathbf{V}}_h^{(d)'} \hat{\boldsymbol{\Delta}}_\Sigma \right) \leq x \right\} \quad \text{and} \quad \mathcal{H}_2(x) = \left\{ 2 P_\alpha^* \left(\hat{\mathbf{V}}_h^{(d)'} \hat{\boldsymbol{\Delta}}_V \mathbf{c} \right) \leq x \right\}. \quad (23)$$

On the set $\mathcal{H}_1(\frac{\lambda}{4}) \cap \mathcal{H}_2(\frac{\lambda}{4})$, we can scale (22) by a factor 2 to obtain

$$2 \left\| \hat{\mathbf{V}}_h^{(d)} (\hat{\mathbf{c}} - \mathbf{c}) \right\|_2^2 + 2 \lambda P_\alpha(\hat{\mathbf{c}}) \leq \lambda P_\alpha(\hat{\mathbf{c}} - \mathbf{c}) + 2 \lambda P_\alpha(\mathbf{c}). \quad (24)$$

We subsequently manipulate $P_\alpha(\hat{\mathbf{c}})$ and $P_\alpha(\hat{\mathbf{c}} - \mathbf{c})$. Using the reverse triangle inequality, we have

$$\begin{aligned} P_\alpha(\hat{\mathbf{c}}) &= \alpha \sum_{g \in \mathcal{G}} \sqrt{|g|} \|\hat{\mathbf{c}}_g\|_2 + (1 - \alpha) \|\hat{\mathbf{c}}\|_1 \\ &\geq \alpha \sum_{g \in \mathcal{G}_S} \sqrt{|g|} \left[\|\mathbf{c}_g\|_2 - \|\hat{\mathbf{c}}_g - \mathbf{c}_g\|_2 \right] + \alpha \sum_{g \in \mathcal{G}_{S^c}} \sqrt{|g|} \|\hat{\mathbf{c}}_g\|_2 + (1 - \alpha) \left[\|\mathbf{c}_S\|_1 - \|\hat{\mathbf{c}}_S - \mathbf{c}_S\|_1 + \|\hat{\mathbf{c}}_{S^c}\|_1 \right] \quad (25) \\ &= P_{\alpha,S}(\mathbf{c}) + P_{\alpha,S^c}(\hat{\mathbf{c}} - \mathbf{c}) - P_{\alpha,S}(\hat{\mathbf{c}} - \mathbf{c}), \end{aligned}$$

where \mathcal{G}_S and \mathcal{G}_{S^c} are defined in Lemma 1. Simple rewriting provides

$$\begin{aligned} P_\alpha(\hat{\mathbf{c}} - \mathbf{c}) &= \alpha \sum_{g \in \mathcal{G}} \sqrt{|g|} \|\hat{\mathbf{c}}_g - \mathbf{c}_g\|_2 + (1 - \alpha) \|\hat{\mathbf{c}}_S - \mathbf{c}_S\|_1 + \alpha \sum_{g \in \mathcal{G}_{S^c}} \sqrt{|g|} \|\hat{\mathbf{c}}_g\|_2 + (1 - \alpha) \|\hat{\mathbf{c}}_{S^c}\|_1 \\ &= P_{\alpha,S}(\hat{\mathbf{c}} - \mathbf{c}) + P_{\alpha,S^c}(\hat{\mathbf{c}} - \mathbf{c}). \end{aligned} \quad (26)$$

Combining results (24)–(26) yields

$$2 \left\| \hat{\mathbf{V}}_h^{(d)} (\hat{\mathbf{c}} - \mathbf{c}) \right\|_2^2 + \lambda P_{\alpha,S^c}(\hat{\mathbf{c}} - \mathbf{c}) \leq 3 \lambda P_{\alpha,S}(\hat{\mathbf{c}} - \mathbf{c}), \quad (27)$$

and $\hat{\mathbf{c}} - \mathbf{c}$ is thus a member of the set $\mathcal{C}_{N_c}(\mathcal{G}, S)$ as defined in Lemma 1. In combination with Lemma 2, thus requiring $\mathcal{H}_1(\frac{\lambda}{4}) \cap \mathcal{H}_2(\frac{\lambda}{4}) \cap \mathcal{V}(\frac{\phi_0}{2})$ to hold, we conclude

$$\begin{aligned} 2 \left\| \hat{\mathbf{V}}_h^{(d)} (\hat{\mathbf{c}} - \mathbf{c}) \right\|_2^2 + \lambda P_\alpha(\hat{\mathbf{c}} - \mathbf{c}) &= 2 \left\| \hat{\mathbf{V}}_h^{(d)} (\hat{\mathbf{c}} - \mathbf{c}) \right\|_2^2 + \lambda P_{\alpha,S}(\hat{\mathbf{c}} - \mathbf{c}) + \lambda P_{\alpha,S^c}(\hat{\mathbf{c}} - \mathbf{c}) \\ &\stackrel{(i)}{\leq} 4 \lambda P_{\alpha,S}(\hat{\mathbf{c}} - \mathbf{c}) \stackrel{(ii)}{\leq} 16 \left\| \hat{\mathbf{V}}_h^{(d)} (\hat{\mathbf{c}} - \mathbf{c}) \right\|_2 \left(\frac{\bar{\omega}_\alpha \lambda}{\phi_0} \right) \stackrel{(iii)}{\leq} \left\| \hat{\mathbf{V}}_h^{(d)} (\hat{\mathbf{c}} - \mathbf{c}) \right\|_2^2 + \frac{64 \bar{\omega}_\alpha^2 \lambda^2}{\phi_0^2}, \quad (28) \end{aligned}$$

where step (i) follows from (27), step (ii) is implied by $P_{\alpha,S}(\hat{\mathbf{c}} - \mathbf{c}) \leq \frac{4\bar{\omega}_0 \|\hat{\mathbf{V}}_h^{(d)}(\hat{\mathbf{c}} - \mathbf{c})\|_2}{\phi_0}$ for $\hat{\mathbf{c}} - \mathbf{c} \in \mathcal{C}_{N_c}(\mathcal{G}, S)$ (Lemma 2), and step (iii) uses the elementary inequality $16uv \leq u^2 + 64v^2$ (i.e. manipulating $(u - 8v)^2 \geq 0$). A straightforward rearrangement of (28) provides the inequality of Theorem 2.

It remains to determine a lower bound on the probability of $\mathcal{H}_1(\frac{\lambda}{4}) \cap \mathcal{H}_2(\frac{\lambda}{4}) \cap \mathcal{Y}(\frac{\phi_0}{2})$. We rely on the elementary inequality $\mathbb{P}(\mathcal{H}_1(\frac{\lambda}{4}) \cap \mathcal{H}_2(\frac{\lambda}{4}) \cap \mathcal{Y}(\frac{\phi_0}{2})) \geq 1 - \mathbb{P}(\mathcal{H}_1(\frac{\lambda}{4})^c) - \mathbb{P}(\mathcal{H}_2(\frac{\lambda}{4})^c) - \mathbb{P}(\mathcal{Y}(\frac{\phi_0}{2})^c)$ to bound the individual probabilities.

We start with $\mathbb{P}(\mathcal{H}_1(\frac{\lambda}{4})^c) = \mathbb{P}(2P_\alpha^*(\hat{\mathbf{V}}_h^{(d)'} \hat{\Delta}_\Sigma) > \frac{\lambda}{4}) \leq \mathbb{P}(\|\hat{\mathbf{V}}_h^{(d)'} \hat{\Delta}_\Sigma\|_\infty > \frac{\lambda}{8})$. The last inequality is true because continuing from (20), we have

$$P_\alpha^*(\mathbf{c}) \leq \alpha \max_{g \in \mathcal{G}} \frac{\|\mathbf{c}_g\|_2}{\sqrt{|g|}} + (1 - \alpha) \|\mathbf{c}\|_\infty \leq \alpha \max_{g \in \mathcal{G}} \frac{\sqrt{|g|} \|\mathbf{c}_g\|_\infty}{\sqrt{|g|}} + (1 - \alpha) \|\mathbf{c}\|_\infty = \|\mathbf{c}\|_\infty \quad (29)$$

for any vector \mathbf{c} . Subsequently, we have

$$\begin{aligned} \mathbb{P}\left(\|\hat{\mathbf{V}}_h^{(d)'} \hat{\Delta}_\Sigma\|_\infty > \frac{\lambda}{8}\right) &= \mathbb{P}\left(\|[(\hat{\mathbf{V}}_h^{(d)} - \mathbf{V}^{(d)}) + \mathbf{V}^{(d)}] \hat{\Delta}_\Sigma\|_\infty > \frac{\lambda}{8}\right) \\ &\leq \mathbb{P}\left(\|\hat{\mathbf{V}}_h - \mathbf{V}\|_1 \|\hat{\Delta}_\Sigma\|_\infty + C_V \|\hat{\Delta}_\Sigma\|_\infty > \frac{\lambda}{8}\right) \leq \mathbb{P}\left(\|\hat{\mathbf{V}}_h - \mathbf{V}\|_{\text{r}}^2 + C_V \|\hat{\mathbf{V}}_h - \mathbf{V}\|_{\text{r}} > \frac{\lambda}{8}\right) \\ &\leq \mathbb{P}\left(\|\hat{\mathbf{V}}_h - \mathbf{V}\|_{\text{r}} > \frac{\lambda^{1/2}}{4}\right) + \mathbb{P}\left(\|\hat{\mathbf{V}}_h - \mathbf{V}\|_{\text{r}} > \frac{\lambda}{16C_V}\right), \end{aligned} \quad (30)$$

exploiting block-diagonality of $\hat{\mathbf{V}}_h^{(d)} - \mathbf{V}^{(d)}$ and $\mathbf{V}^{(d)}$ such that $\|\hat{\mathbf{V}}_h^{(d)} - \mathbf{V}^{(d)}\|_1 = \max_{1 \leq i \leq N} \|\hat{\mathbf{V}}_{i,h} - \mathbf{V}_i\|_1 \leq \|\hat{\mathbf{V}}_h - \mathbf{V}\|_{\text{r}}$ and $\|\mathbf{V}^{(d)}\|_1 \leq \|\mathbf{V}\|_{\text{r}} \leq C_V$ (Assumption X). Bounds for the final RHS terms in (30) are available from Theorem 1.

Second, we have

$$\begin{aligned} \mathbb{P}\left(\mathcal{H}_2\left(\frac{\lambda}{4}\right)^c\right) &\leq \mathbb{P}\left(\|\hat{\mathbf{V}}_h^{(d)'} \hat{\Delta}_V \mathbf{c}\|_\infty > \frac{\lambda}{8}\right) \leq \mathbb{P}\left(\|\hat{\mathbf{V}}_h^{(d)'} [\hat{\mathbf{V}}_h^{(d)} - \mathbf{V}^{(d)}]\|_\infty > \frac{\lambda}{8\|\mathbf{c}\|_\infty}\right) \\ &\leq \mathbb{P}\left(\|\hat{\mathbf{V}}_h - \mathbf{V}\|_1 \|\hat{\mathbf{V}}_h - \mathbf{V}\|_\infty + C_V \|\hat{\mathbf{V}}_h - \mathbf{V}\|_\infty > \frac{\lambda}{8\|\mathbf{c}\|_\infty}\right) \\ &\leq \mathbb{P}\left(\|\hat{\mathbf{V}}_h - \mathbf{V}\|_{\text{r}} > \frac{\lambda^{1/2}}{4}\right) + \mathbb{P}\left(\|\hat{\mathbf{V}}_h - \mathbf{V}\|_{\text{r}} > \frac{\lambda}{16C_V}\right), \end{aligned} \quad (31)$$

where the last line relies on the union bound and the fact that $\|\mathbf{c}\|_\infty < 1$ (implied by Assumption 1). Hence, the sets $\mathcal{H}_1(\frac{\lambda}{4})^c$ and $\mathcal{H}_2(\frac{\lambda}{4})^c$ admit the same probability bound.

Finally, $\mathbb{P}(\mathcal{Y}(\frac{\phi_0}{2})^c) = \mathbb{P}(\|\hat{\mathbf{V}}_h - \mathbf{V}\|_1 > \frac{\phi_0}{2}) \leq \mathbb{P}(\|\hat{\mathbf{V}}_h - \mathbf{V}\|_{\text{r}} > \frac{\phi_0}{2})$. Combining all previous results, we conclude

$$\begin{aligned} &\mathbb{P}\left(\mathcal{H}_1\left(\frac{\lambda}{4}\right) \cap \mathcal{H}_2\left(\frac{\lambda}{4}\right) \cap \mathcal{Y}\left(\frac{\phi_0}{2}\right)\right) \\ &\geq 1 - 2\mathbb{P}\left(\|\hat{\mathbf{V}}_h - \mathbf{V}\|_{\text{r}} > \frac{\lambda^{1/2}}{4}\right) - 2\mathbb{P}\left(\|\hat{\mathbf{V}}_h - \mathbf{V}\|_{\text{r}} > \frac{\lambda}{16C_V}\right) - \mathbb{P}\left(\|\hat{\mathbf{V}}_h - \mathbf{V}\|_{\text{r}} > \frac{\phi_0}{2}\right) \\ &\geq 1 - 5\mathbb{P}\left(\|\hat{\mathbf{V}}_h - \mathbf{V}\|_{\text{r}} > 6f(\lambda, \phi_0)\right), \end{aligned} \quad (32)$$

where $f(\lambda, \phi_0) = \min\left(\frac{\lambda^{1/2}}{24}, \frac{\lambda}{96C_V}, \frac{\phi_0}{12}\right)$. The proof is completed by evaluating the final probability in (32) with the use of Theorem 1. \square

Proof of Corollary 1. First, we derive the conditions under which the set on which the performance bound in Theorem 2 holds occurs with probability converging to one. Under Assumption 2(b1), along with the remaining assumptions in Theorem 2, this probability is given by $1 - \mathcal{P}_1(f(\lambda, \phi_0), N, T)$, where we recall from Theorem 1 that

$$\begin{aligned} \mathcal{P}_1(f(\lambda, \phi_0), N, T) = N^2 & \left(b_1 T^{(1-\delta)/3} + \frac{[2h(f(\lambda, \phi_0), N) + 1]b_3}{f(\lambda, \phi_0)} \right) \exp\left(-\frac{T^{(1-\delta)/3}}{2b_1^2}\right) \\ & + \frac{b_2 N^2 [2h(f(\lambda, \phi_0), N) + 1]^d}{f(\lambda, \phi_0)^d T^{\frac{\delta}{2}(d-1)}} \end{aligned} \quad (33)$$

Given that $\lambda \in O(T^{-q_\lambda})$ with $q_\lambda > 0$, it follows immediately that

$$f(\lambda, \phi_0) = \min\left(\frac{\lambda^{1/2}}{24}, \frac{\lambda}{96C_v}, \frac{\phi_0}{12}\right) = O(T^{-q_\lambda}). \quad (34)$$

In addition, following the remark below Theorem 1, it holds that

$$h\left(\frac{\lambda}{96C_v}, N\right) = O\left(\log\left(\frac{N}{\lambda}\right)^2 k_0\right) = O(\log(T)^2 T^{q_k}). \quad (35)$$

Based on (34) and (35), it follows that the first RHS-term in (33) converges to zero exponentially in T for any $\delta < 1$. The second RHS-term, however, converges to zero at most at a polynomial rate. Accordingly,

$$\mathcal{P}_1(f(\lambda, \phi_0), N, T) = O\left(\frac{N^2 [h\left(\frac{\lambda}{96C_v}, N\right) + 1]^d}{\lambda^d T^{\frac{\delta}{2}(d-1)}}\right) = O\left(\log(T)^{2d} T^{2q_N + dq_k + dq_\lambda - \frac{\delta(d-1)}{2}}\right), \quad (36)$$

where the second equality holds from the observation that for any $\delta < 1$ the first two RHS terms in the first equality converge to zero at an exponential rate, whereas the third term may converge to zero at most at a polynomial rate. From (36), it follows that $\mathcal{P}_1(f(\lambda, \phi_0), N, T) \rightarrow 0$ if

$$2q_n + dq_k + dq_\lambda - \frac{\delta(d-1)}{2} < 0 \Rightarrow q_\lambda < -\frac{2q_n}{d} - q_k + \frac{\delta(d-1)}{2d}.$$

In a similar fashion, we derive the conditions under which $\mathcal{P}_2(f(\lambda, \phi_0)) \rightarrow 0$, by noting that

$$\begin{aligned} \mathcal{P}_2(f(\lambda, \phi_0), N, T) = N^2 & \left[\frac{\beta_1 [2h(f(\lambda, \phi_0), N) + 1]}{f(\lambda, \phi_0)} + \frac{2}{\beta_2} \left(\frac{Tf(\lambda, \phi_0)^2}{[2h(x, N) + 1]^2} \right)^{\frac{1}{7}} \right] \times \\ & \exp\left(-\frac{1}{\beta_3} \left(\frac{Tf(\lambda, \phi_0)^2}{[2h(f(\lambda, \phi_0), N) + 1]^2} \right)^{\frac{1}{7}}\right) \end{aligned} \quad (37)$$

converges to zero exponentially fast in T if $\frac{Tf(\lambda, \phi_0)^2}{[2h(f(\lambda, \phi_0), N) + 1]^2}$ diverges at a polynomial rate in T . Making use of (34) and (35), it follows that

$$\frac{Tf(\lambda, \phi_0)^2}{[2h(f(\lambda, \phi_0), N) + 1]^2} = O(\log(T)^{-4} T^{1-2q_\lambda-2q_k}),$$

which translates to the condition

$$1 - 2q_\lambda - 2q_k > 0 \Rightarrow q_\lambda < \frac{1}{2} - q_k.$$

This establishes conditions (i) and (ii) in Corollary 1.

We proceed by deriving the order of the performance bound in Theorem 2. Noting that

$$\sum_{g \in \mathcal{G}_S} \sqrt{|g|} \leq |\mathcal{G}_S| \max_{g \in \mathcal{G}_S} \sqrt{|g|} = O\left(T^{q_g + q_N/2}\right),$$

it follows that

$$\bar{\omega} = O\left((1 - \alpha)T^{q_g + q_N/2} + \alpha T^{q_S/2}\right).$$

Then, by Theorem 2,

$$\left\| \hat{\mathbf{V}}_h^{(d)}(\hat{\mathbf{c}} - \mathbf{c}) \right\|_2^2 \leq \frac{4\bar{\omega}_\alpha^2 \lambda^2}{\phi_0^2} = O\left((1 - \alpha)T^{2q_g + q_N - 2q_\lambda} + \alpha T^{q_S - 2q_\lambda}\right)$$

and

$$(1 - \alpha) \sum_{g \in \mathcal{G}} \sqrt{|g|} \|\hat{\mathbf{c}}_g - \mathbf{c}_g\|_2 + \alpha \|\hat{\mathbf{c}} - \mathbf{c}\|_1 \leq \frac{4\bar{\omega}_\alpha^2 \lambda}{\phi_0^2} = O\left((1 - \alpha)T^{2q_g + q_N - q_\lambda} + \alpha T^{q_S - q_\lambda}\right),$$

on a set with probability $1 - \mathcal{P}_1(f(\lambda, \phi_0), N, T)$ or $1 - \mathcal{P}_2(f(\lambda, \phi_0), N, T)$, depending on whether Assumption 2(b1) or 2(b2) applies, respectively. Since we have shown that both $\mathcal{P}_1(f(\lambda, \phi_0), N, T) \rightarrow 0$ and $\mathcal{P}_2(f(\lambda, \phi_0), N, T) \rightarrow 0$ under the conditions imposed in Corollary 1, the proof is complete. \square

Appendix C Empirical Application: Additional Material

C.1 Satellite data

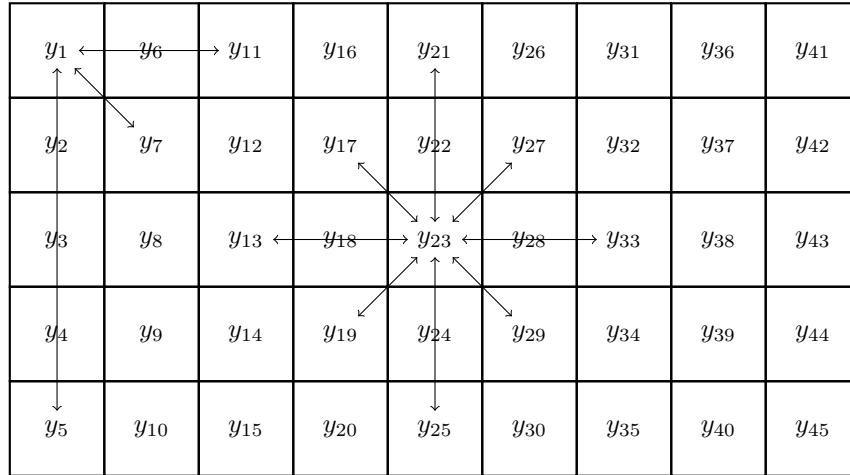


Figure 5: Vertically ordered spatial grid. The arrows display part of the admissible interactions for spatial units y_1 and y_{23} under the identification constraint that spatial units y_i, y_j may only interact if $|i - j| < \lfloor N/4 \rfloor = 11$.

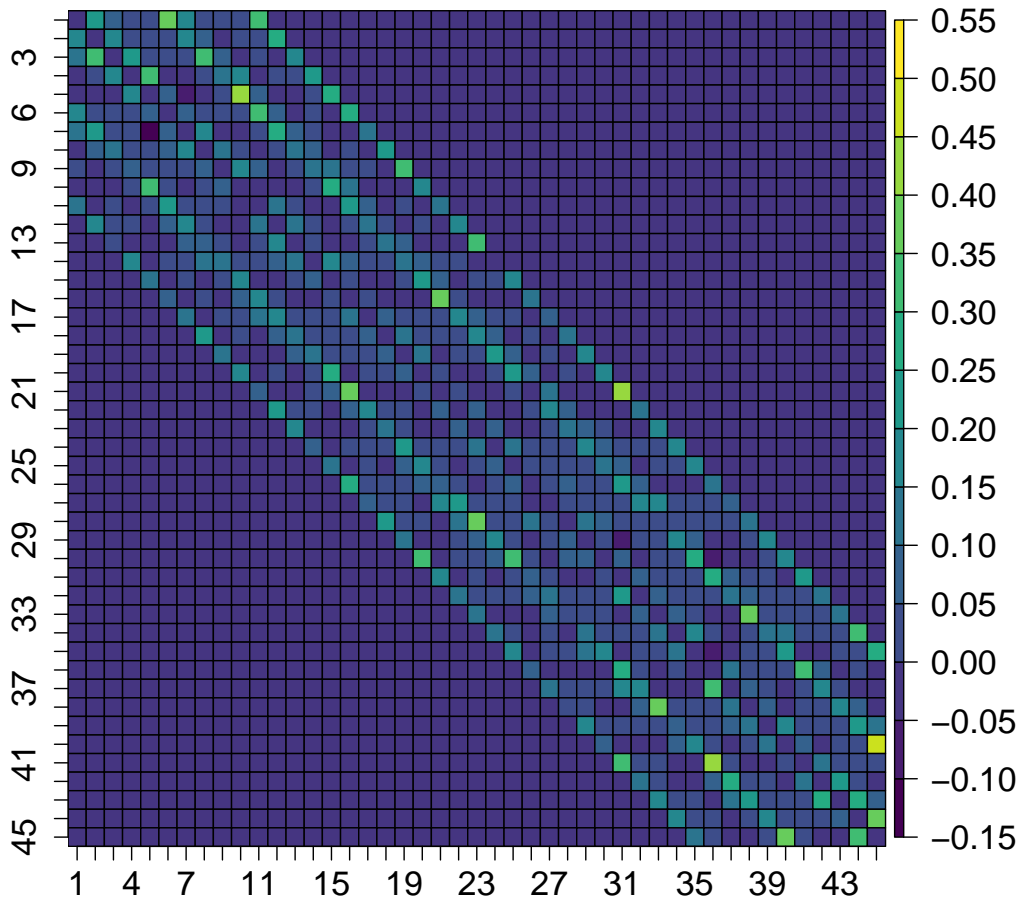


Figure 6: The coefficient sizes estimated by $\text{SPLASH}(0, \lambda_{CV})$. While there is no sparsity within the admissible bandwidth, the diagonal that were estimated zero by λ_{AIC} are estimated close to zero.